

## Fixed Wing Team 3: Final Engineering Design Report

Supervisor: Shane Windsor

TA: Rafael Heeb

### Team SwiftSky

Name	Role
Avinash Ashok	Project Manager; Flight Dynamics & Control
Lingges Shaswat	Chief Engineer; Landing Gear and Fuel Systems
Tanveer Talokder	Structures & Manufacturing
Patricia Mihailovici	Operational Performance & Propulsion
Jason Francis	Aerodynamics
Dara Murray	Business, Economics & Operability
Bjork Elezi	Systems and CAD

### ABSTRACT

This report documents Fixed Wing Team 3's (SwiftSky) final aircraft design. The overall goal of this project was to design a 170-passenger in a 2-class configuration commercial aircraft with a 4200 NM maximum range that would reduce direct operating costs for the airline by 15% against its competitors. Market research was conducted as well as analysis of the specification to form a set of design drivers and objectives for the aircraft design, from which six initial concepts were conceived and evaluated. The final design chosen was an aircraft with a low-mounted, swept, high-aspect ratio wing with the addition of folded wing tips. Three design iterations were completed, resulting in an aircraft with an MTOW of 99 Tonnes, an AR of 12 and cruise Mach of 0.82. An overall reduction of operating costs of 6% was achieved against the A321neo - the failure to reach the 15% objective was attributed mainly to the engine operating outside of its design range and the early EIS date of 2030, rendering the use of novel concepts implausible.

## NOMENCLATURE & SYMBOLS

Table 1: Table of nomenclature

Acronym/Symbol	Meaning
ACN	Aircraft Classification Number
ADS-B	Automatic Dependent Surveillance–Broadcast
AFRP	Aramid Fibre Reinforced Polymer
APU	Auxiliary Power Unit
AR	Aspect Ratio
AVL	Athena Vortex Lattice
$C_{D0}$	Parasite (zero lift) drag coefficient
$C_L$	Lift coefficient
CFRP	Carbon Fibre Reinforced Polymer
CoG	Centre of Gravity
COC	Cash Operating Cost
DOC	Direct Operating Cost
ECS	Environmental Control System
EIS	Entry Into Service
EMA	Electro-Mechanical Actuator
EPNdB	Effective Perceived Noise in Decibels
EVS	Enhanced Vision System
FDR	Final Design Review
FEDR	Final Engineering Design Report
GFRP	Glass Fibre Reinforced Polymer
GPWS	Ground Proximity Warning System
HD	High Density
HLD	High Lift Devices
HTP	Horizontal Tail Plane
HUD	Head Up Display
ICAO	International Civil Aviation Organization
INS	Inertial Navigation System
ISA	International Standard Atmosphere
LE	Leading Edge
MEA	More Electric Architecture
MLW	Maximum Landing Weight
MLG	Main Landing Gear
MWE	Manufacturers Weight Empty
MRW	Maximum Ramp Weight
MTOW	Maximum Take-off Weight
MZFW	Maximum Zero Fuel Weight
NLG	Nose Landing Gear
NRC	Non-Recurring Cost
OEI	One Engine Inoperative
OWE	Operational Weight Empty
pax	Passengers
PDR	Preliminary Design Review
PEDR	Preliminary Engineering Design Report
RC	Recurring Cost
RCT	Rear Centre Tank
RDTE	Research, Development, Test & Evaluation
RNP	Required Navigation Performance
RoC	Rate-of-Climb
RPU	Remote Power Unit
SLS	Sea Level Static
TCAS	Traffic Collision Avoidance System
TE	Trailing Edge
TRL	Technology Readiness Level
TRU	Transformer Rectifier Unit
VSCF	Variable Speed Constant Frequency
VTP	Vertical Tail Plane

## CONTENTS

### I Configuration

<b>1 Executive Summary</b>	<b>5</b>
<b>2 General Arrangement</b>	<b>7</b>
<b>3 Aircraft Data Sheet</b>	<b>8</b>
<b>4 Cabin Layout</b>	<b>9</b>
<b>5 Market Analysis &amp; Requirements</b>	<b>9</b>
5.1 Market Research . . . . .	9
5.2 Estimated Sales . . . . .	11
5.3 Requirements & Objectives . . . . .	11
5.4 Design Drivers . . . . .	11
<b>6 Concept Selection &amp; Justification</b>	<b>11</b>
6.1 Initial Concepts . . . . .	11
6.2 Concept Down Selection . . . . .	12
6.3 Detailed Design Trade-offs . . . . .	13
<b>7 Final Design</b>	<b>14</b>
7.1 Wing . . . . .	14
7.2 Empennage . . . . .	15
7.3 Wing Structure . . . . .	15
7.4 Materials and Manufacturing . . . . .	16
7.5 Weight, Balance & Stability . . . . .	16
7.6 Propulsion and Performance . . . . .	17
7.7 Landing Gear . . . . .	17
<b>8 Economic Analysis</b>	<b>18</b>
8.1 Operating Cost Breakdown . . . . .	18
8.2 Recurring and Non-Recurring Costs . . . . .	18
8.3 Break Even Analysis . . . . .	18
8.4 Sensitivity Study of MSP and Fuel Price . . . . .	19
<b>9 Operability</b>	<b>20</b>
9.1 Turnaround Time . . . . .	20
<b>10 Aircraft Characteristics vs Specification</b>	<b>20</b>
<b>11 Technology Levels &amp; Risk Analysis</b>	<b>21</b>
11.1 Technology Readiness Levels . . . . .	21
11.2 Economic Risk Analysis . . . . .	21
11.3 Technological Risk Analysis . . . . .	22
11.4 Environmental Impact . . . . .	23
<b>12 Critical Analysis of Design &amp; Way of Working</b>	<b>23</b>
12.1 Critical Analysis of Design . . . . .	23
12.1.1 Landing Gear Design . . . . .	23
12.1.2 Aerodynamics . . . . .	23
12.1.3 Folding Wing Tip . . . . .	23
12.2 Way of Working & Team Management . . . . .	23

<b>13 Conclusion</b>	<b>24</b>
----------------------	-----------

## II Technical Description

<b>14 Systems</b>	<b>25</b>
14.1 Electrical Systems . . . . .	25
14.2 Avionics . . . . .	26
14.3 Fuel Systems . . . . .	26
14.4 Folding Wing Tip . . . . .	26
<b>15 Weight, Stability &amp; Control</b>	<b>27</b>
15.1 Weight Breakdown . . . . .	27
15.2 CoG calculations . . . . .	28
15.3 Stability & Control . . . . .	29
<b>16 Structures &amp; Manufacturing</b>	<b>29</b>
16.1 Wing Structures . . . . .	29
16.2 Material Selection . . . . .	31
16.3 Manufacturing . . . . .	33
<b>17 Aerodynamics</b>	<b>34</b>
17.1 Wing Design . . . . .	34
17.2 Aerofoil & Cruise Performance . . . . .	34
17.3 High Lift Design . . . . .	35
17.4 Drag . . . . .	36
<b>18 Landing Gear</b>	<b>37</b>
18.1 Configuration and Integration . . . . .	37
18.2 Design Philosophy . . . . .	37
18.3 Final Design . . . . .	37
18.4 Tyre Sizing . . . . .	38
18.5 Brake Sizing . . . . .	38
18.6 Shock Absorber and Material Analysis . . . . .	38
<b>19 Propulsion &amp; Performance</b>	<b>39</b>
19.1 Engine Scaling . . . . .	39
19.2 Engine Position . . . . .	39
19.3 Take-off and Landing . . . . .	39
19.4 Cruise Performance . . . . .	41
19.5 Noise . . . . .	42

## Part I

# Configuration

### 1 EXECUTIVE SUMMARY

In recent years, medium/long-range, narrowbody aircraft have emerged as a popular choice for airlines as they offer a versatile and efficient solution to meeting the needs of modern air travel. Their ability to cover substantial, intercontinental routes whilst maintaining cost effectiveness gives them high operational flexibility and adaptability to a variety of market conditions. As carriers strive to optimise their fleets and enhance overall performance, they are increasingly investing in this type of aircraft. Boeing and Airbus currently dominate the market with their 737 MAX series and A320neo family - these aircraft families have become extremely popular amongst airlines and are manufactured at high rates.

SwiftSky's objective was to design a competitor aircraft that would occupy a market gap by reducing the aircraft's operating cost by 15% when compared to its competitors (in particular, the Airbus A321neo). In line with the specification laid out by Airbus [1], the aircraft was designed to: carry 170 passengers in a 2-class configuration, have a design range of 4200 *NM*, adhere to ICAO Code C limits, and enter into service in 2030.

As the primary design driver was to minimise the operating costs, a number of key factors were focused on throughout the design process: lowered fuel costs through high aerodynamic efficiency; increased utilisation by reducing transit time and turnaround time; lightweight and structurally efficient airframe through optimal use of composite materials; lowered research-, development- and manufacturing-costs in order to price the aircraft competitively whilst maximising profits; and easy airframe- and engine-maintenance. The final design for the SwiftSky aircraft was a conventional set-up with low-wing, underwing-mounted engines, conventional low-tail empennage and the addition of a folding wing-tip mechanism to increase the wingspan whilst adhering to the 36 *m* gate limit. Two initial variants have been presented - the 170-passenger, 2-class layout (S170) and a 222-passenger, high-density, 1-class layout (S222).

During the design, considerations have been made for family developments of the aircraft to reduce future development costs and increase market share by covering a larger range of air travel requirements. This includes the removal/addition of RCTs to decrease/increase range, along with the shortening/extension of the cabin to decrease/increase the passenger capacity. By allowing for these changes, carriers can benefit from shared components, technologies, and cabin crew/pilot training, resulting in streamlined operations and reduced costs.

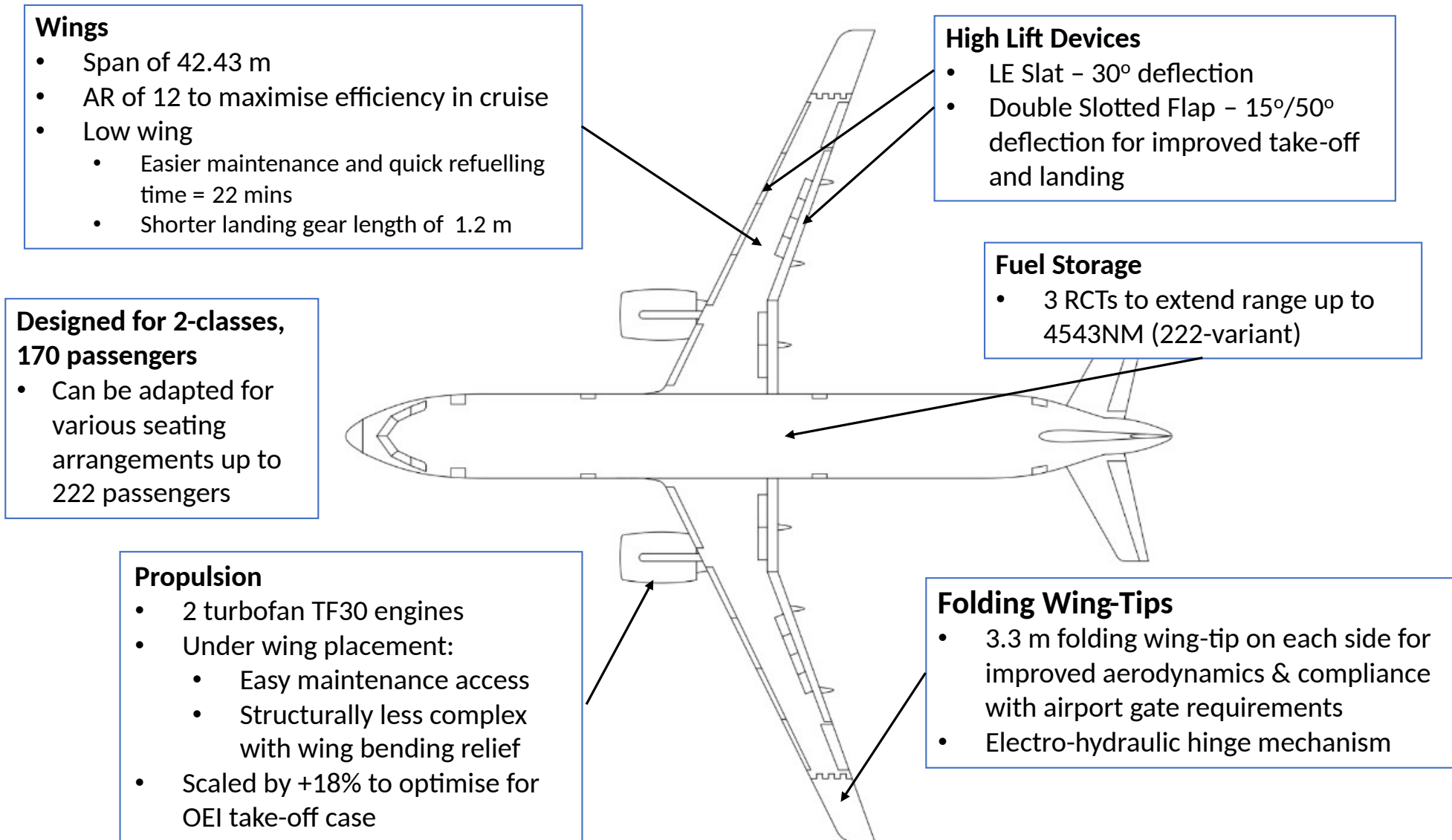
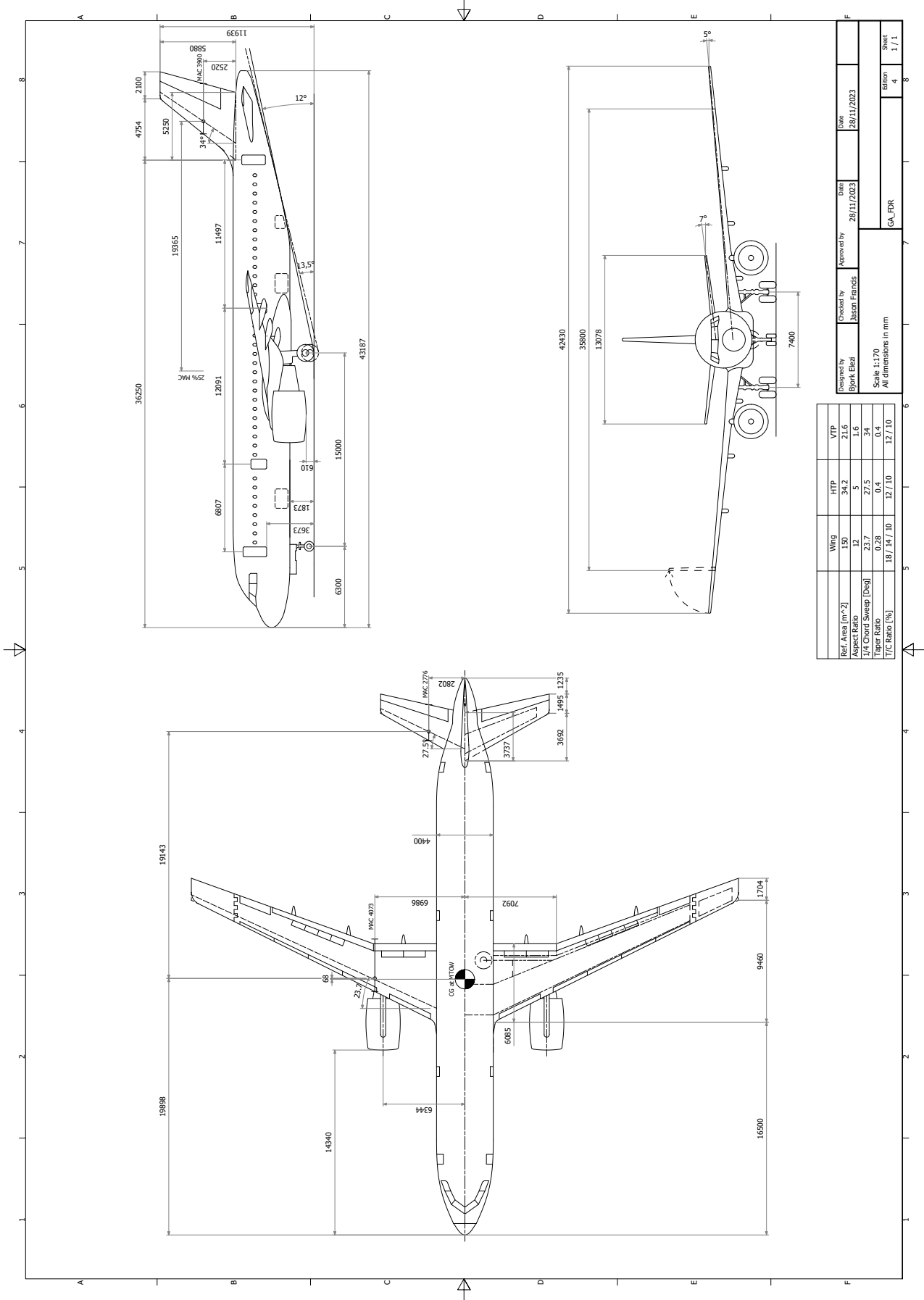


Figure 1: SwiftSky walkarounds chart

## 2 GENERAL ARRANGEMENT



### 3 AIRCRAFT DATA SHEET

Item	Value	Units	Additional Comments
Configuration	Conventional with Folding Wing Tips		
Maximum Take-Off Mass	98909	kg	High Density Layout
Operators Weight Empty	47040	kg	High Density Layout
Fuel for design mission 4200 nm (including reserves)	27943	kg	
Fuel for 3000 nm (excluding reserves)	14697	kg	
Payload for design mission	17850	kg	2-Class Design Mission (not including crew)
Maximum Landing Mass	84073	kg	
Maximum Zero Fuel Mass	69381.00	kg	
Maximum Fuel Capacity	29528.00	kg	
Cruise Mach No	0.82		
VCr/MCr (VCr in kts CAS)	261/0.82	kts CAS / - Cr = Cruise	
Initial Cruise Altitude	35000	ft	
L/D (at start of Cruise for 4200 nm mission)	20.05		
Take-Off Field Length	1600.68	m	OEI condition - at sea level (Design Mission)
Landing Field Length	1925.26	m	At sea level (Design Mission)
Approach Speed	137	kts	
Fuselage Length	43.19	m	
Diameter	4.4	m	
Wing Area	150.0	m^2	
Span	42.43	m	
Aspect Ratio	12		
Thickness of Wing @ outer wing (t/c)	0.1		
Taper Ratio	0.28		
Mean Aerodynamic Chord	4.073	m	
Sweep @ 1/4 Chord	23.7	degs	
High Lift System (trailing edge)	Double Slotted Flap		
High Lift System (leading edge)	Slat		
Cmax at landing	2.91		
Distance of wing LE at root from nose	16.5	m	
Distance of wing MAC from datum (specify datum)	6.984	m	Fuselage Centreline
Tailplane Area	34.2	m^2	
Span	13.08	m	
Aspect Ratio	5		
1/4 Chord MAC (wing) to 1/4 Chord MAC (tailplane)	19.143	m	
Fin Area	21.6	m^2	
Span	5.88	m	
Aspect Ratio	1.6		
1/4 Chord MAC (wing) to 1/4 Chord MAC (fin)	19.365	m	
Number of Engines	2		
Engine position (wing/fuselage/other)	under wing		
Thrust (per Engine) Sea Level Static	35409.11	lbf	
Engine Thrust Scale Factor	1.18		
Engine or fan diameter	1.92	m	
sfc at mid cruise 3000 nm mission	0.026	lbm/hr/lbf	
Landing Gear Layout	Retractable Tricycle		
Main Landing Gear Tyre Size	52x20.5R20	inches	*Goodyear Tyres
Main Landing Gear Geometry for ACN	1212	mm	*Leg Length
ACN	52.7		COMFAA Tool
Height of Fuselage Datum above Ground	5.5	m	*To fuselage centreline
CG range at MTOM	5.4	% MAC	
Aircraft NRC	2800	Million \$	Using Roskam's method
Aircraft RC	50	Million \$	Based on estimated number of aircraft built of 2950
Manufacture's Study Price	126	Million \$	Scaled by existing commercial aircraft cost and MTOW
Engine Price (per engine)	12.5	Million \$	Scaled by exiting turbofan engine cost and thrust
Aircraft DOC	47,400	\$/trip	Based on study mission, HD layout
Turnaround time	51.8 / 37 / 38.5	mins	1-Class Layout (Scenario 1 / Scenario 2 / Scenario 3)
Refuel time	22 / 16	mins	Design Mission / Study Mission
Trim Tank yes/no	No		

## 4 CABIN LAYOUT

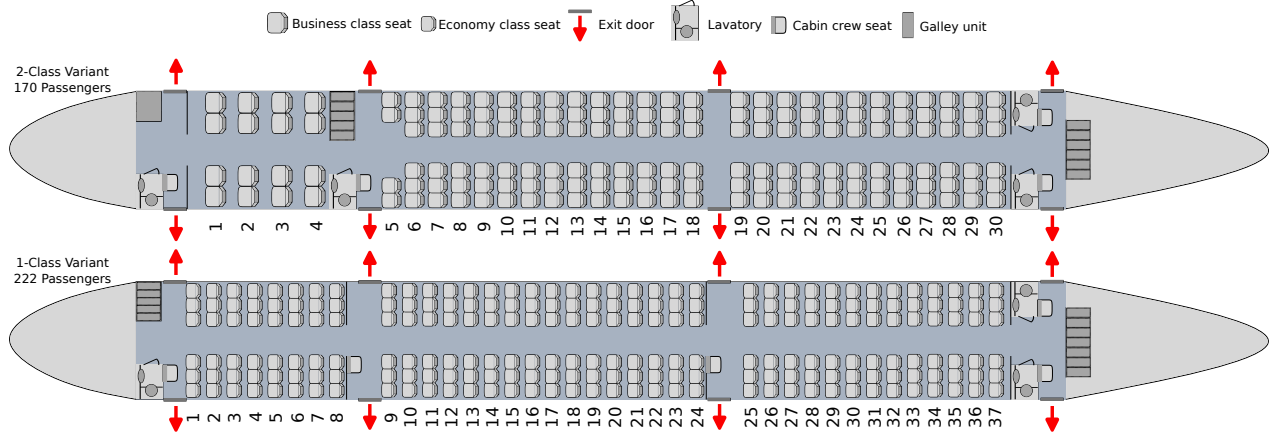


Figure 2: SwiftSky cabin layouts

SwiftSky has developed two initial possible cabin layouts for an airliner to choose from: a 170-passenger, 2-class layout, and a 222-passenger, 1-class, HD layout. To maximise the use of space in the aircraft, a single aisle,  $3 \times 3$  layout was chosen. Table 2 shows a breakdown of items for each layout.

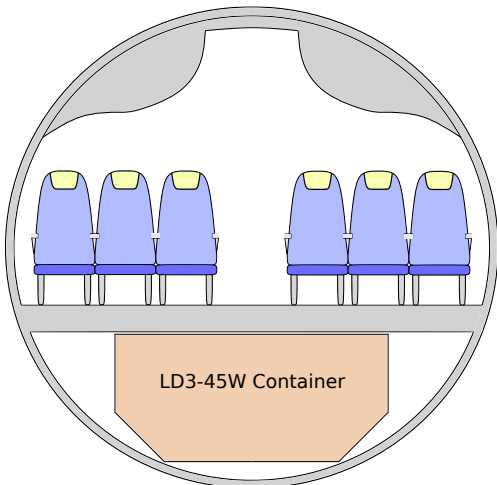


Figure 3: Cabin cross section

To satisfy the emergency evacuation requirement for both layouts the aircraft has a total of eight type C exits. At the front and rear of the cabin on either side, there are modified type C exits ( $72'' \times 30''$ ) - these are taller than standard to assist with passenger entry and exit as they are the primary doors. In front of, and behind the main wing there are standard-sized type C emergency exits on each side of the cabin ( $48'' \times 30''$ ).

There are two cargo holds, each consisting of 4 LD3-45W containers - one at the front, and one at the rear of the aircraft.

## 5 MARKET ANALYSIS & REQUIREMENTS

### 5.1 Market Research

Market research has been conducted on the current commercial aircraft industry in order to assess any potential gaps in the market, shown in Figure 4. It was found that airlines are increasingly investing in low-cost carriers (LCCs), with the focus on lower direct operating costs, higher aircraft utilisation

and higher passenger load factors [2]. For a newly designed aircraft, it is imperative that these factors are at the forefront of the design process if the aircraft is to capture significant market share.

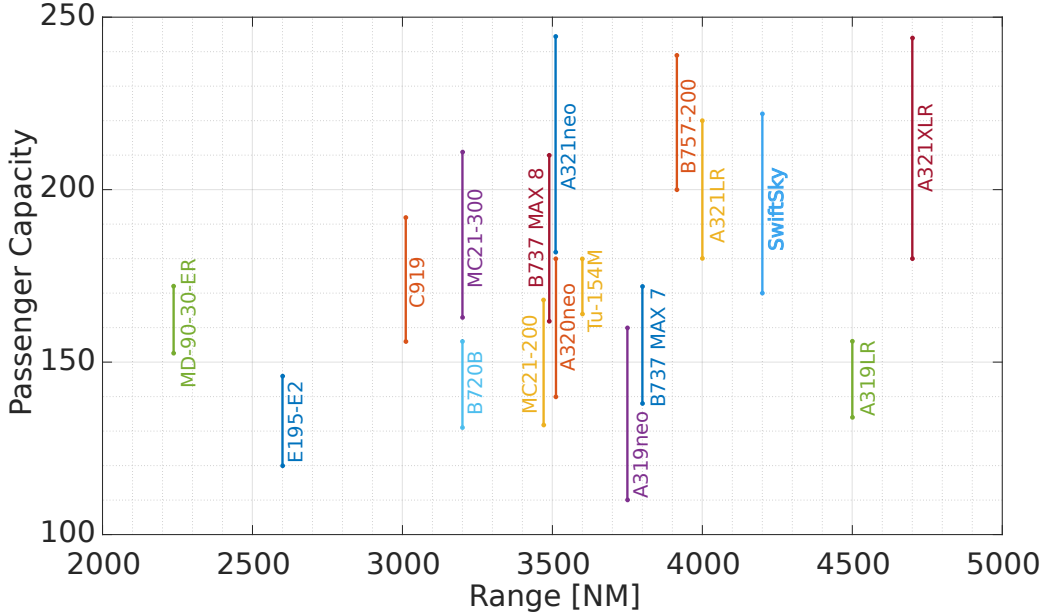


Figure 4: Commercial aircraft passenger capacities and range

Figure 5 shows the payload range of the SwiftSky 170-variant compared to its closest competitors. Its maximum range is 4254 NM carrying a payload of 170 passengers, while the A321neo has a lower maximum range of 3995 NM [3] for 180 passengers. The same goes for the A321LR, with a maximum range of 4000 NM for 206 passengers [4]. The SwiftSky high-density variant is compared to the A321XLR [5], having a 3.5% lower range for 2 more passengers.

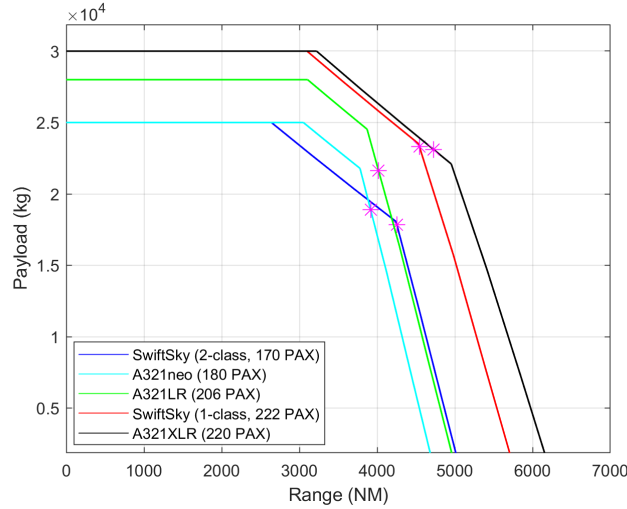


Figure 5: SwiftSky payload-range diagram compared to competitor aircraft

In response to the air travel market's evolving needs, the SwiftSky aircraft will occupy a notable gap in the market (Figure 4) due to its high versatility and economic efficiency. With reduced operating costs against its competitors, long maximum range and flexible passenger capacity, it will fulfil any airline's need for high utilisation, high passenger load factor and economical operation.

## 5.2 Estimated Sales

Based on Airbus [6] and Boeing [7] sales forecasts for 2023-42, an estimate for single-aisle passenger aircraft sales was calculated for 2030-44. The market dominance of medium-long-range aircraft within the single-aisle category was then evaluated using Airbus order and deliveries figures [8], and a model, based on A321neo figures, was created to estimate the market capture for a new narrowbody aircraft. This original model accounts for the phasing-out of the A321neo as they are replaced by the new, more efficient SwiftSky aircraft. The model predicts that market share starts low, rising to a maximum of 25% by the year 2038 after which the share begins to drop slightly to account for newer aircraft models being introduced. It is estimated conservatively that over the 14-year period, a total number of 2950 aircraft will be sold. This was validated by looking at order numbers for the A321neo (5530 since EIS 2017 [8]) and the 737 MAX (5903 since EIS 2017 [9]). This confirmed the validity of our sales estimate.

## 5.3 Requirements & Objectives

The project specification [1] was assessed to identify requirements and objectives. These provided the basis of the design drivers and selection criteria for the SwiftSky aircraft. They are summarised in Table 3.

Table 3: Summary of requirements and objectives

Hard requirements	Soft requirements	Objectives
ICAO Code C	Cruise altitude	Airframe life $\geq$ 25 years
4200 NM range	Cruise speed	Minimise turn-around time ( $\leq 50\text{mins}$ )
Take-off & landing field length		Minimise weight
Min. 170 pax		2030 entry into service
		-15% lower DOC than A321neo

## 5.4 Design Drivers

The main goal of this design is to achieve a 15% reduction in DOC compared to the A321neo. To attain this objective, the design was guided by several key drivers:

- 1. Aerodynamic Efficiency:** The aircraft was designed for optimum aerodynamic efficiency, directly reducing fuel burn and hence DOC. This approach makes the design more robust with respect to future fluctuations in fuel prices. The aerodynamics were optimised through trade studies on major wing parameters.
- 2. Operations:** The aircraft's layout was designed for minimising turnaround time and hence increasing the number of flights per day. Cruise speed and altitude were driven by the lowest block time to increase utilisation.
- 3. Manufacturing:** The aircraft manufacturing and material selection was driven by reducing cost without compromising on aerodynamic efficiency and weight. The manufacturing methods and overall design complexity were also aimed to achieve an EIS of 2030.
- 4. Future Development:** The aircraft was designed with scope for the development of different variants so that the aircraft can be made adaptable to market changes.

## 6 CONCEPT SELECTION & JUSTIFICATION

### 6.1 Initial Concepts

The design concepts considered for the project are sketched in Figure 6. The conventional concept (Figure 6a) has the benefit of high design maturity and manufacturing simplicity. By adding a folding wing-tip to the conventional design (Figure 6b), the induced drag will decrease with the increase of aspect ratio, thus improving fuel efficiency, while still complying with the standard airport requirements.

This concept comes with the disadvantage of increased weight and structural complexity associated with the hinge mechanism.

By having a 3-engine configuration (Figure 6c), the aircraft will benefit from better OEI (one-engine-inoperative) handling and smaller engines can be used. However, this implies an increased overall weight, extra maintenance needed, increased fuel consumption and cabin noise.

The Double-Bubble, Blended Wing and Box Wing concepts (Figures 6d, 6e, 6f) all come with the benefit of improving aerodynamic efficiency, at the expense of increased structural complexity. The low maturity of their design is a key factor that needs to be considered, as the Entry into Service in 2030 goal needs to be fulfilled.

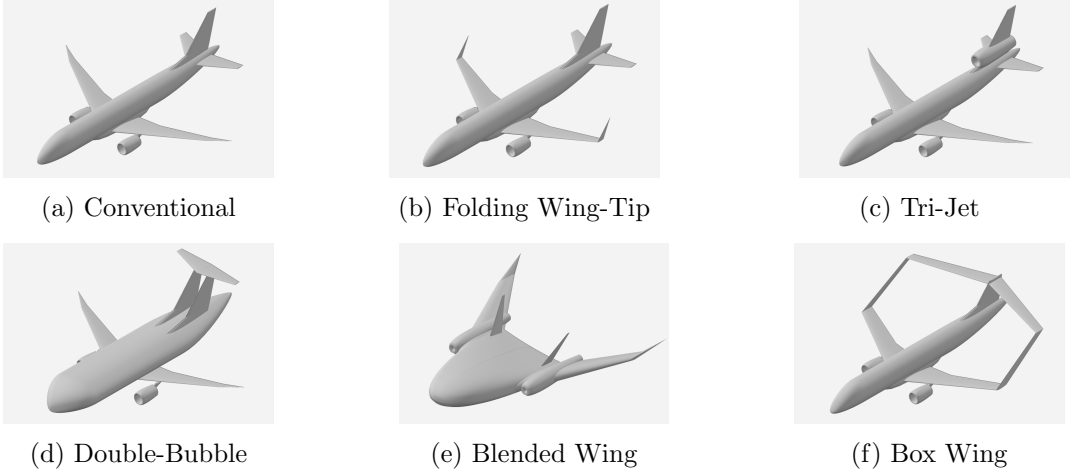


Figure 6: Design concepts

## 6.2 Concept Down Selection

From the specification and the hard requirements identified several key design factors were chosen as ranking criteria to judge the initial concepts. They were each given a justified weighting out of 10 shown in Table 4.

Table 4: Concept down selections criteria

Criteria	Weight (1-10)	Justification
Development & Manufacturing cost	6	Higher cost means less profit margin for same MSP
Maintenance cost	10	Direct driver of DOC
Crew training cost	6	Drives DOC but one time investment only
Airframe efficiency	7	Drives weight hence fuel burn
Control & stability	3	Conform to regulations, uncomplicated manoeuvres
Evacuation	7	Certification impacts feasibility of novel ideas
Engine failure	5	Drives engine sizing and hence fuel consumption
Fuel efficiency	10	Direct driver of DOC
Passenger comfort	3	Only need to meet requirements
Turnaround time	8	Drives number of flights per day and hence DOC
Service life	9	Lower annual expenses reduce fixed cost in DOC
Cruise performance	8	Drives fuel burn as most fuel burnt in cruise
Take-off & Landing Performance	5	Meet requirements, drives engine sizing and weight
Noise	3	Only need to meet requirements

A Pugh matrix was used to down-select the initial concepts against the criteria in Table 4. Concept

(a), a conventional-style aircraft, was selected as the baseline because the technology and design are mature and are widely used in the industry, so any new concept must be justified to be better than the conventional design concept for its introduction into the industry. Every other concept was scored between -2 and 2, with the negative scores being inferior to concept (a) and positive meaning superior to concept (a).

Table 5: Concept down selection sub-group 1/sub-group 2

Criteria	Weight	A	B	C	D	E	F
Development & manufacturing cost	6	0/0	-1/0	-1/-1	-2/-2	-2/-2	-2/-2
Maintenance cost	10	0/0	-1/-1	-2/-1	0/0	-2/-2	-1/0
Crew training cost	6	0/0	0/0	0/0	-1/0	-2/-2	-1/-1
Airframe efficiency	7	0/0	0/-1	-1/-1	0/-1	-2/-2	-1/-2
Control & stability	3	0/0	0/0	1/1	0/-1	-2/-1	-1/1
Evacuation	7	0/0	0/0	0/0	-1/-1	-2/-2	0/0
Engine failure	5	0/0	1/0	2/2	0/0	-1/-2	1/-1
Fuel efficiency	10	0/0	1/1	-1/-2	2/1	2/1	1/2
Passenger comfort	3	0/0	0/0	0/0	1/1	-1/1	0/0
Turnaround time	8	0/0	0/0	-1/-1	0/0	-1/-1	0/0
Service life	9	0/0	0/0	0/-1	-1/-1	-1/-2	0/-1
Cruise performance	8	0/0	1/1	-2/-1	1/2	2/2	1/1
Takeoff & Landing performance	5	0/0	1/1	2/1	1/1	-1/1	-1/1
Noise	3	0/0	0/0	-2/-1	1/0	2/0	0/0
<b>TOTAL</b>		0/0	<b>12/6</b>	-50/-53	5/-4	-66/-77	-20/-10

The team split into two sub-groups and the groups conducted the scoring separately, this removed some bias from the down-selection process. Both teams independently concluded that concept (b) was the highest-scoring option that would meet the objectives of the project. Concept (d) was found to be the second highest scoring, but this design is complex and novel, so would be challenging to get it into service by 2030. A sensitivity study was performed by adjusting the weighting of the significant criteria by  $\pm 10\%$  to validate the robustness of our study and ensure that small changes in the weight assigned to each criterion do not significantly alter the outcome. It was again found that concept (b) scored highest. A matrix is shown in Table 5 where the '/' represents the score from each sub-group.

### 6.3 Detailed Design Trade-offs

Existing aircraft were researched to assess the advantages and disadvantages of wing, engine and empennage arrangements. This informed trade studies on wing placement, engine placement, empennage configuration and a span reduction system. Table 6 is the trade study for span reduction systems between actuated hinge folding wing tips, passive hinge folding wing tips, telescopic wing tips and a variable-sweep wing where each design has been ranked 4 to 1 with 4 being best (ranked the same if equal). An actuated hinge wing tip was selected.

Table 6: Span reduction trade study

Criteria	Weight (1-5)	Actuated hinge	Passive hinge	Telescopic	Variable sweep
Ease of maintenance	5	4	4	1	2
Weight	3	4	3	2	1
Aero. efficiency	4	3	4	3	1
Fuel storage	4	4	4	1	2
Reliability	5	4	3	1	1
Manoeuvrability	1	2	4	2	4
Passenger experience	2	4	1	3	2
Ground safety	2	4	2	1	4
<b>TOTAL</b>		<b>98</b>	86	42	46

In the trade studies (Appendix), a low-wing design was chosen over mid and high placements due to its advantages in easier maintenance access for quicker turnarounds and improved aerodynamic efficiency over high wing) for fuel-efficient cruising. The limited ground clearance for a low wing was the configuration's main drawback as this limits the maximum engine intake hence the bypass ratio and engine efficiency. The engine will be placed under the wing for easier maintenance access for ground crews, structural simplicity, and reduced weight compared to over-wing or rear fuselage placement. The conventional low-tail empennage was chosen over T-tail, V-tail, H-tail, and cruciform configurations due to its lighter weight, improved control surface access for maintenance and moderate aerodynamic efficiency.

## 7 FINAL DESIGN

### 7.1 Wing

The SwiftSky aircraft features a low-mounted, swept, high aspect ratio wing for optimal cruise performance. This design prioritises minimising fuel consumption while simultaneously providing flexibility for future variant development. An AR of 12 was chosen through a trade study, detailed in Figure 7, which considered DOC as a function of wing weight, aerodynamic fuel efficiency, design complexity, manufacturing cost, and maintenance cost/time. Optimisation studies were performed on other wing parameters such as twist and taper ratio which are discussed in section 17. The wing thickness varies from 18% at the root to 10% at the tip, representing a compromise on aerodynamics as increased thickness facilitates easier landing gear integration, wing box integration, and maximisation of fuel storage within the wings. This configuration allows for increased fuel tank capacity in the fuselage, allowing the development of longer-range variants. For an overview of the final wing parameters, please refer to Table 7.

Table 7: Wing Geometry

Parameter	Value
Area [ $m^2$ ]	150.0
Span [m]	42.43
Aspect Ratio	12
Taper	0.28
MAC [m]	4.073
1/4 Chord Sweep [ $^\circ$ ]	23.7
Twist [ $^\circ$ ]	-2
Setting Angle [ $^\circ$ ]	1.0
Dihedral [ $^\circ$ ]	5

Table 8: Aerodynamic Characteristics

Parameter	Value
Cruise $C_L$	0.581
Cruise $L/D$	20.05
$C_{LMax}$ Landing	2.91
$C_{LMax}$ Take-off	2.82

Table 9: HTP & VTP Geometry

Parameter	HTP	VTP
Area [ $m^2$ ]	34.2	21.6
Span [m]	13.08	5.88
Aspect Ratio	5	1.6
Taper	0.4	0.4
MAC [m]	2.776	3.900
Setting angle [ $^\circ$ ]	-1.7	0.0

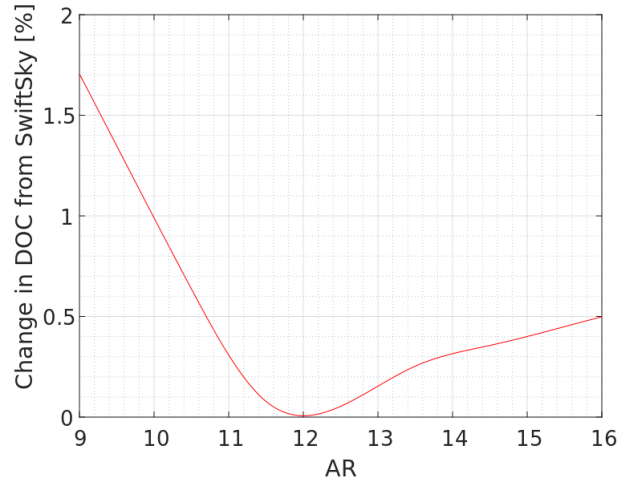


Figure 7: AR optimisation against DOC

The aircraft operates at an average lift coefficient in cruise of 0.581 at  $M = 0.82$  this drove the choice for the NASA Phase 2 SC(2)-06XX aerofoil series to be selected due to its 0.6 design lift coefficient and supercritical design [10]. The wing was swept to  $23.7^\circ$  so that drag divergence occurs at  $M = 0.84$  and does not impede cruise performance. MIT's AVL software (a vortex lattice method) was used to assess cruise performance with an additional wave drag addition from Lock [11] as AVL only applies a linearly compressible correction. This defined that the necessary setting angle of the wings to be  $1^\circ$

for optimum cruise performance giving an L/D cruise of 20.05.

SwiftSky has an HLD system consisting of a 10% chord length LE slat and a 25% chord length TE double-slotted flap with maximum deflections of 30° and 50° respectively. The slat is across 75% of the span and the flap 60% of the span. This configuration provides a  $C_{LMax} = 2.91$  in its landing configuration which exceeds the necessary lift for the aircraft to land at MLW at stall speed, this ensures that if new variants have an increased weight the HLD system does not need to be redesigned.

## 7.2 Empennage

HTP and VTP areas were initially sized using Sadraey's tail volume coefficients [12]. Placement ensured that both surfaces' main spars intersected the fuselage aft of the cabin bulkhead, with empennage parameters detailed in Table 9. Verification was conducted using AVL to ensure the meeting of OEI take-off and stability in trim requirements. The HTP incorporates a supercritical SC(2)-0012 aerofoil to minimise drag from compressibility effects during cruise. The aircraft was trimmed for zero pitching moment in the cruise condition, resulting in an HTP setting angle of  $-1.7^\circ$ . Control surfaces were sized using Sadraey's method [12] and verified in AVL to meet CS 25.147 [13], Table 10 summarises the sizing.

Table 10: Control surface sizing

Surface	Span fraction [%]	Chord fraction [%]	Max Deflection [°]
Aileron	20	30	25
Elevator	80	30	30
Rudder	80	30	25

## 7.3 Wing Structure

The wing design is shown in Figure 8. It consists of two wing boxes, one in the main section and another in the folding wing tip, leaving enough gap for the hinge and actuator mechanism. The wing boxes are designed with two spars, ribs and skin stiffened with stringers, which altogether resist the primary loads of the wing. The LE is 13% of the chord, while the TE is 32% of the chord (Figure 9). The height of the wing box is 18% of the chord at the root, which reduces linearly to 10% at the tip. The most extreme load case of  $2.5g$ , an ultimate safety factor of 1.5 [14] and a material knockdown factor of 1.14 [15] were used to size the structural components of the wing. The wing box in the folding wing tip does not store any fuel.

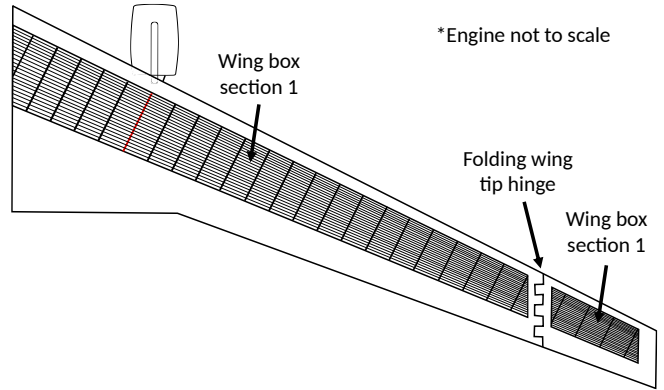


Figure 8: Top view of wing showing the two wing box sections with the ribs, stringers, and engine mounted on the 6th rib (highlighted in red)

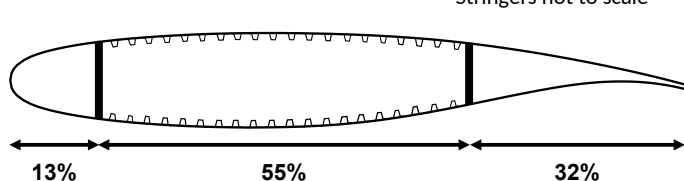


Figure 9: Wing cross section showing hat stringers and wing box width as percentage of chord

As a result, it was concluded that 20 hat stringers will be needed in one skin panel with the spacing between them reducing along the span from 119.0 mm at the root to 48.8 mm at the tip (Figures 8 and 9). 26 ribs are needed in the design with a fixed spacing of 686 mm, which ensures the engine is mounted on the 6th rib (Figure 8). The thickness of both spars is equal and it varies along the span as shown in Figure 10. Similarly, the upper and lower skin panels have equal thicknesses and vary along the span as shown in Figure 11.

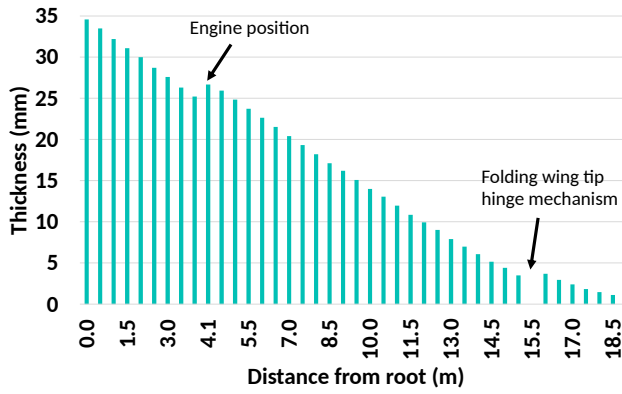


Figure 10: Main wing spar thickness variation along the span



Figure 11: Wingbox skin thickness variation along the spar

## 7.4 Materials and Manufacturing

The fuselage and LE of the main wing are made of the AA2524-T3 aluminium alloy. The LE of the VTP is made of GFRP, while the nose cone is made of AFRP. The rest of the structural components such as the main wing, HTP and VTP are made of CFRP. Titanium will be used for the folding wing hinge. The composite parts are made using the resin transfer infusion (RTI) method. Stringers will be infused together with the skin in one step with high-density closed-shell foam structures, rather than using bonding adhesives or fasteners - Figure 30. Overall, the aircraft's structural weight will consist of 50% composites as shown in Figure 12.

## 7.5 Weight, Balance & Stability

The aircraft has an MTOW of 98909 kg (S222 variant). The OWE is 47 tonnes, with the remaining weight consisting of fuel, payload and operational items. The S222 has a design payload of 23825 kg, with passengers, baggage, and crew included. The S170 has a design payload of 18380 kg with fewer passengers and one less crew member. The front and rear cargo holds can each carry 2331 kg with LD3-45W containers at 85% volumetric filling density. The remaining weight is allocated to fuel for the design missions. The typical CoG at take-off is 29% MAC for S222 and 37% MAC for S170.

The aircraft's fuel capacity is 29528 kg, with the S170 and S222 requiring 24943 kg and 27943 kg for a 4200 NM range, including reserves. The RCT stores 6815 kg of jet fuel, while the wings, including centre tanks, hold up to 22713 kg. To minimise the impact on flight stability, the RCTs were placed at 22 m from the nose.

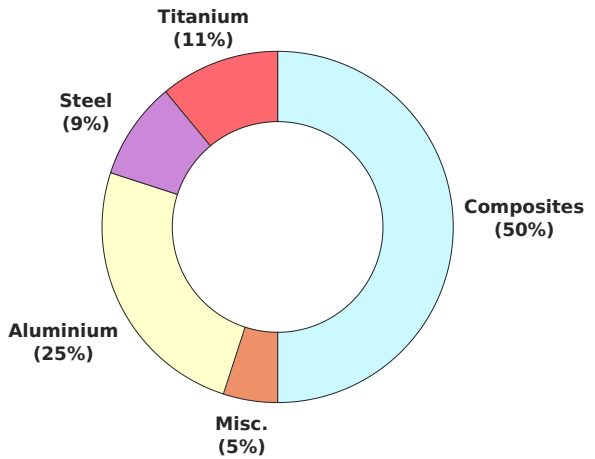


Figure 12: Material usage percentage breakdown

## 7.6 Propulsion and Performance

The 2 turbofan TF30 engines are scaled using a thrust scaling factor of +18%, being limited by the OEI take-off distance requirement. For the design mission of 4200 NM, the aircraft is cruising at Mach 0.82 using the step climb technique in 4 steps, from an initial cruise altitude of 35,000 ft to the final altitude of 41,000 ft. The mission profile diagram can be observed in Figure 13, while a mission characteristics breakdown of each phase can be found in Table 26 in the appendix.

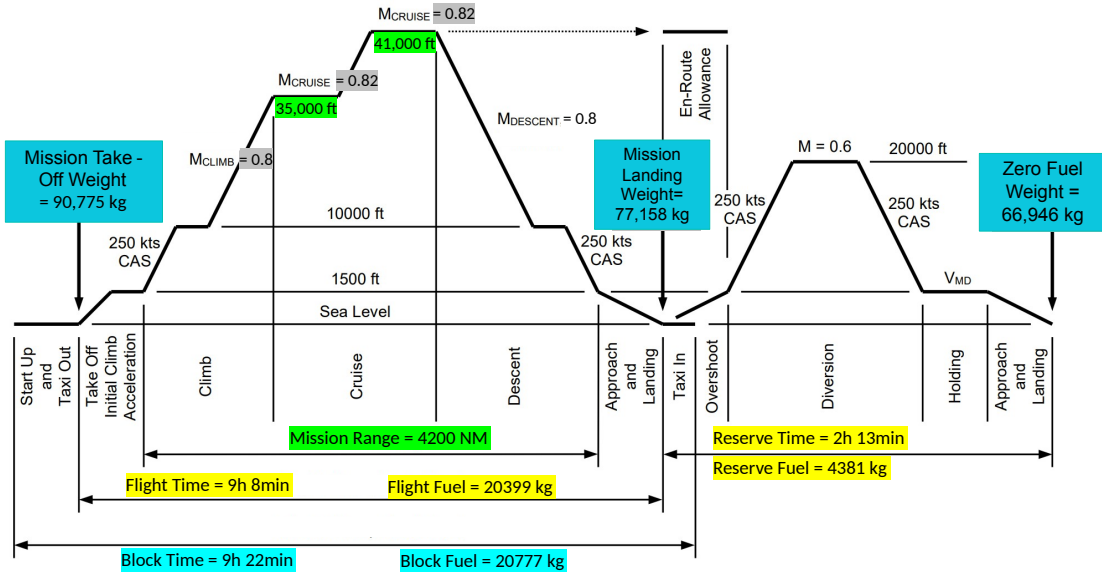


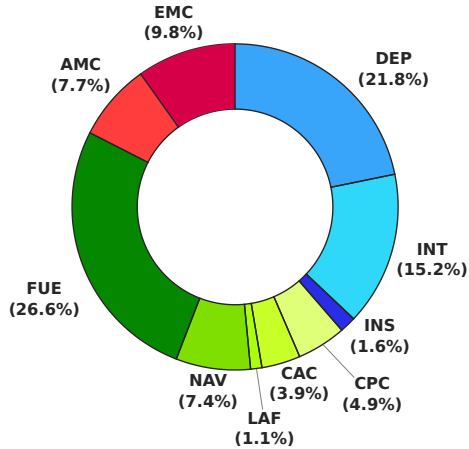
Figure 13: Mission profile diagram

## 7.7 Landing Gear

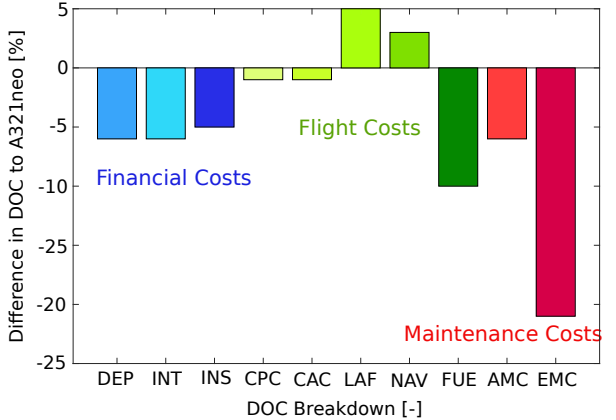
To lower turnaround times, a retractable tricycle configuration was chosen as it enables quicker loading and unloading of passengers and cargo. A single-strut twin-wheel NLG that retracts forward into the fuselage and a two-strut twin-wheel MLG that retracts into the wing was designed to withstand the highest load share possible. For the MLG, 20" carbon brakes were used with radial Goodyear tyres sized 52x20.5R20 as they absorb the aircraft's kinetic energy. Runway limits were considered to size and position the landing gear ensuring ground stability, steering capability, tail-strike angle and ground clearance. The components of the landing gear shall be made from titanium and steel alloys as it provides a good compromise between cost, strength and weight.

## 8 ECONOMIC ANALYSIS

### 8.1 Operating Cost Breakdown



(a) DOC breakdown



(b) A321neo comparison

Figure 14: DOC for High Density Configuration

The AEA method [16] has been used to calculate DOCs for the SwiftSky aircraft as well as competitor aircraft for comparison. The MSP figure of \$125,000,000 for the aircraft was scaled against existing commercial aircraft by MTOW, and the engine price of \$12,600,000 was scaled against existing turbofan engines by maximum thrust. Figure 14a shows the DOC breakdown for the high-density configuration of the SwiftSky aircraft. Flight costs account for the majority of the direct operating costs (43.9%), followed by financial costs (38.6%) and maintenance costs (17.5%). Overall a 6% reduction in DOC was achieved against the A321neo.

### 8.2 Recurring and Non-Recurring Costs

The Roskam method [17] has been used to calculate RCs and NRCs. The NRCs are made up of research, development, testing and evaluation costs and the entire project is estimated as \$2.8 billion. The RC is the cost of manufacturing one aircraft and is dependent on the number of aircraft produced. For the estimated sales figure of 2950, the RC is \$50 million.

It is important to note the limitations of the Roskam method due to its age - the figures it produces are useful estimates but should be validated using existing aircraft data, however, such data is not generally openly available. FlightGlobal [18] claims that the development costs for the A320neo were around \$1.3 billion. Although more data is required, this suggests that the \$2.8 billion is fairly accurate as the A320neo project was primarily an aircraft redesign, and was for EIS 2016. Although no exact data can be found for the manufacturing cost of competitor aircraft, it is estimated that the A321neo costs around \$40 million to manufacture, validating the Roskam estimate.

### 8.3 Break Even Analysis

Using the RCs from Roskam methods and the calculated MSP figure, estimations for break-even numbers have been calculated. The minimum number of aircraft that must be produced to be able to break even is 84, at which point 83 sales would result in breaking even. After this point the break-even number drops as the number of aircraft produced increases. At the estimated sales figure of 2950, 43 sales are required to break even. In reality, the aircraft would not be sold at MSP - discounts would be offered to airlines. Given a 10% markup (selling at \$55 million), 560 aircraft sales would be required. If the sales estimate is reached, the break-even number is likely to be in between these two figures.

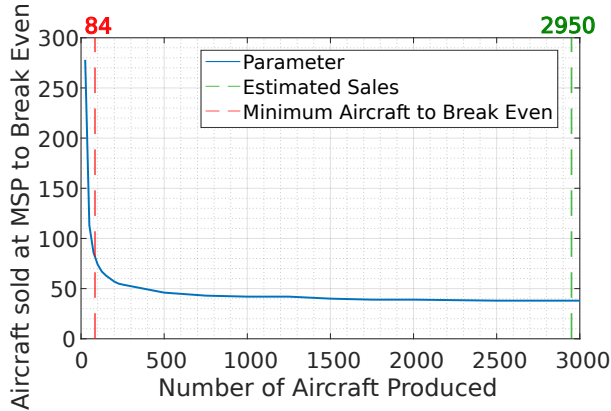
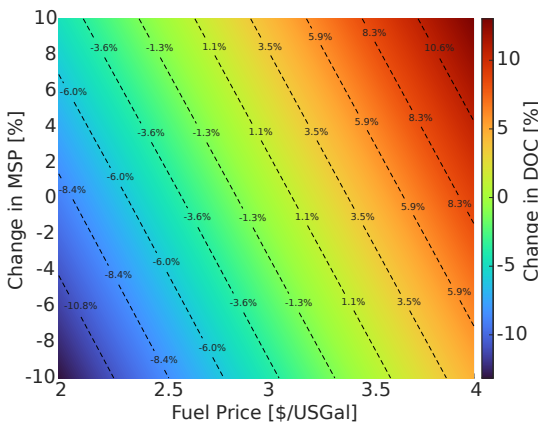


Figure 15: Number of aircraft produced vs breakeven number

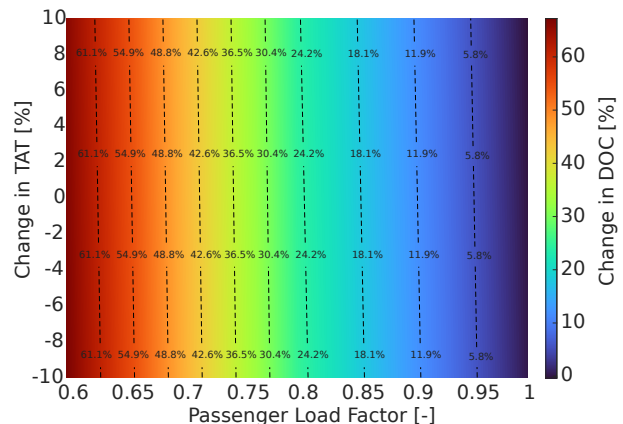
#### 8.4 Sensitivity Study of MSP and Fuel Price

It is important to consider the fluidity of the economic market when calculating operating costs. Changes in market demand will affect the MSP of the aircraft, and fuel prices can change dramatically over the lifetime of an aircraft. Therefore, a sensitivity study has been completed to assess the change in direct operating cost as a result of changes to the MSP and fuel prices - this can be seen in Figure 16a. It can be seen that even small changes in fuel price can increase the DOC significantly, however, due to the higher fuel efficiency of the SwiftSky aircraft compared to its competitors, it will be less affected by fuel price fluctuations.

A study was also completed on the effect of passenger load factor and change in turnaround time on the DOC - see Figure 16b. A turnaround time change of  $\pm 10\%$  was considered to account for airport differences and unforeseen delays - this has minimal effect on the DOC, however, reductions in the passenger load factor have a very strong effect. As the SwiftSky aircraft has a lower passenger capacity than the A321neo in the HD layout, it increases the likelihood of achieving a high passenger load factor, making it more desirable for airlines.



(a) MSP and fuel price



(b) Turnaround time and passenger load factor

Figure 16: Sensitivity studies for DOCs

These results show a robust response to a variety of market variations for the SwiftSky aircraft - even in times of economic downturn when air travel is less popular, it will still be profitable to run.

## 9 OPERABILITY

### 9.1 Turnaround Time

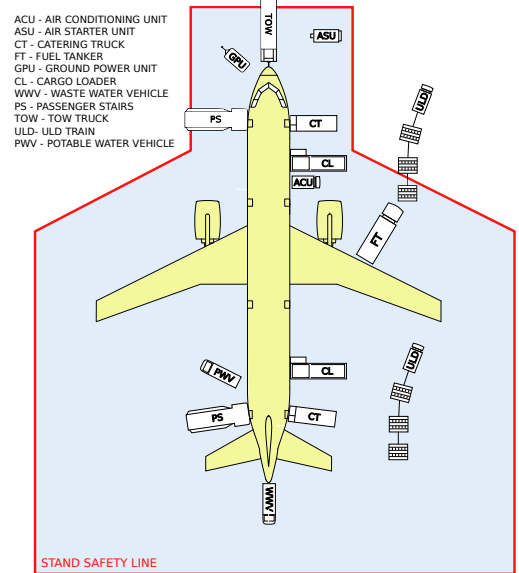
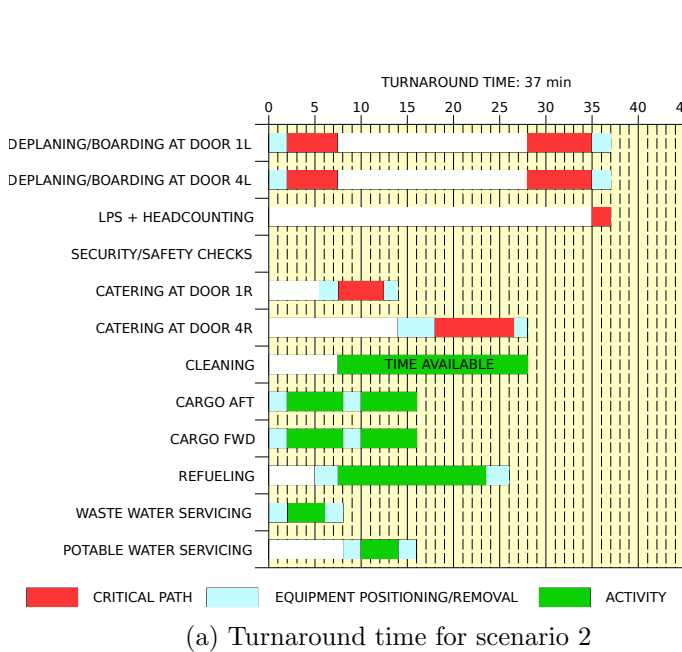


Figure 17: SwiftSky turnaround time and ramp layout

By reducing turnaround time, the overall utilisation of the aircraft can be increased, lowering operating costs, and therefore increasing profitability. As such, the aircraft has been designed to minimise turnaround time. The three turnaround scenarios outlined by the specification have been considered:

- Full 1-class passenger payload changeover including baggage, catering and water/waste at a standard single airport jetway, no refuelling.
- Full 1-class passenger payload changeover including baggage, catering and water/waste on an open apron, no refuelling.
- Full 1-class passenger payload changeover including baggage, catering and water/waste on an open apron, refuelling for a design mission flight.

The critical paths for each case have been evaluated, and times of 51.8 min, 37 min and 38.5 min respectively have been calculated. The refuelling time for the design mission was calculated as 22 min. The full list of turnaround time assumptions can be found in the appendix.

To decrease the turnaround time in each case an outside-in method [19] will be implemented to reduce boarding time. Catering galleys have been placed near to the doors on the starboard side, and all cargo is to be stored in cargo containers, rather than bulk storage.

The aircraft is designed to be capable of operating fully with only existing airport infrastructure. Figure 17b shows a typical ramp layout for a full-service turnaround (Scenario 3).

## 10 AIRCRAFT CHARACTERISTICS VS SPECIFICATION

Table 11 summarises a comparison between the original requirements from the specification and the SwiftSky aircraft. All requirements were met by the design configuration except for only achieving a 6% reduction in DOC. This is attributed to the engine that had to be significantly scaled up moving it out of its optimal performance range. The EIS date of 2030 further constrained the DOC as it meant that any novel concepts were unfeasible.

Table 11: Summary of the key requirements and the achieved performance

Requirements	Units	Target	SwiftSky
Passenger Capacity (2-class MR rules)	-	170	170
Passenger Capacity (1-class HD rules)	-	-	222
Design Range	NM	4200	4238
Study Mission Scenario	NM	3000	3000
Cruise Speed	Mach	-	0.82
Time To Climb (1500ft to ICA at ISA)	mins.	$\leq 30$	28
Initial Cruise Altitude (at ISA)	ft	$\geq 33000$	35000
Maximum Cruise Altitude	ft	$\geq 41000$	41000
Approach speed (MLW, S-L, ISA)	kts CAS	$\leq 140$	137
Take Off Field Length (MTOW, S-L, ISA+15)	m	$\leq 2500$	1600.28
Landing Field Length (MLW, S-L, ISA)	m	$\leq 2200$	1925
OEI Cruise Altitude	ft	-	23400
MMO	Mach	-	0.84
Equivalent Cabin Altitude (at Cruise)	ft	8000	8000
Turn-Around Time	mins.	-	37
DOC Target	\$/seat-NM	A321neo -15%	-6%
Expected Entry Into Service	year	2030	2030

## 11 TECHNOLOGY LEVELS & RISK ANALYSIS

### 11.1 Technology Readiness Levels

Due to regulations set in place by EASA and the FAA, in order to achieve the EIS 2030 objective, it was decided that all technologies to be used for the SwiftSky aircraft should have a TRL of 8 or higher as of 2023. The European Union definition for TRLs [20] was used as a standard for the project.

Aircraft components that have not reached a sufficient TRL will not be considered for the initial EIS of the aircraft to remain on schedule, however, will be reviewed for a potential future retrofit or integration into a family development.

Table 12: TRLs for potential SwiftSky technologies

Aircraft Technology	TRL	Notes
Folding Wing-Tips	9	Used on the Boeing 777X
Electric Taxiing System	7	eTAXI in development by Safran
Resin Infusion Composite Manufacturing	9	Used on the Airbus A220 wing
Hydrogen Fuel Cell	5	Airbus ZEROe in development - EIS 2035
Electric Propulsion	7	Demonstrated in smaller aircraft
Bio-Composites	4	Used in non-aerospace applications
Transonic Laminar Flow Wing	7	Airbus BLADE Demonstration
Additive Composite Manufacturing	9	Used extensively in industry for small parts

### 11.2 Economic Risk Analysis

Undertaking an aircraft design project always comes with a large economic risk. Economic cycles, environmental regulation and geopolitical changes can all have a significant effect on market demand. From the risk analysis conducted (Table 13), economic hazards can be better avoided due to the mitigations put in place.

Table 13: SwiftSky economic risk analysis (L = Likelihood (/5), I = Impact (/5), S = Severity ( $L \times I$ )) (Yellow = 1-8, Orange = 9-16, Red = 17-25)

Risk	L	I	S	Mitigations
Fuel price fluctuation	4	2	8	SwiftSky aircraft has been designed to be robust to market fluctuations - its fuel efficiency and competitive MSP will ensure it's relative DOC (in comparison to competitor aircraft) will remain low.
Runaway development costs	3	3	9	Strong project management and financial discipline throughout RDTE phase. Close collaboration with suppliers, customers, and regulatory bodies.
Failure to reach projected sales figures	3	2	6	Sales forecast is estimated conservatively and cross-checked against data from Airbus and Boeing. Aircraft is priced so that the project will still be profitable at far lower sales than the estimate.
Failure to achieve EIS date	3	2	6	Removal of technologies with a TRL of 7 and lower.

### 11.3 Technological Risk Analysis

Table 14: SwiftSky technological risk analysis (L = Likelihood (/5), I = Impact (/5), S = Severity ( $L \times I$ )) (Yellow = 1-8, Orange = 9-16, Red = 17-25)

Risk	L	I	S	Mitigations
Failure to actuate wing tip	1	4	4	The wing tip mechanism has been designed with redundancy to ensure any failure does not result in a catastrophic failure. The locking mechanism is designed so that, if power is cut off, the wing tip is locked in its extended position.
Difficulty in RCT maintenance	3	2	6	Aircraft designed for easy access to the fuel tanks. Development of a comprehensive maintenance plan. Thorough crew training on the intricacies of servicing.
Composite material compatibility issues leading to delamination or reduced bond strength	3	3	9	Adherence to composite engineering regulations and extensive static testing phase to ensure material compatibility.
Failure to certify skin-stringer infusion method	4	1	4	Planning and execution of an intensive testing program. Close collaboration with regulatory bodies. If the method cannot be certified in time, a conventional method will be used.

Due to the maturity of the conventional aircraft design, the major technological risks were instead centred around the newer components and manufacturing methods used. The technological risk analysis (Table 14) conducted along with relevant mitigations will be used to reduce the likelihood of any potential technological failures.

## 11.4 Environmental Impact

As aviation authorities are becoming increasingly stricter on environmental sustainability and emissions standards, the SwiftSky has been designed to minimise any negative environmental impact. To future-proof the design, the SwiftSky aims to not only adhere to regulations but to surpass them significantly. A number of methods have been used to achieve this:

- Design for low fuel consumption.
- Capability to run on jet fuel blend with a high percentage of SAF.
- Efficient manufacturing processes to reduce waste.
- End-of-life considerations - reuse and recycling of parts.
- Optimised profile descent (OPD) to reduce noise.

# 12 CRITICAL ANALYSIS OF DESIGN & WAY OF WORKING

## 12.1 Critical Analysis of Design

### 12.1.1 Landing Gear Design

The landing gear was sized for a 15% increase of MTOW and is over-engineered for the required aircraft. Previous aircraft that were modified to fly further and carry more weight did not take family extension into account and that is why these manufacturers always had to redesign and resize the landing gear for it to be able to handle the extra weight during landing. Redesigning the landing gear takes up 12% of total aircraft development costs which are within tens of billions of dollars [21]. This could have been mitigated if future family extensions were not considered.

### 12.1.2 Aerodynamics

Upon review after the final design iteration it became apparent our design had a greater wing thickness and less sweep than that of the 757-200 [22] and A321 [23] whilst cruising at slightly higher Mach numbers. This discrepancy suggests the need for more validation that the design is suitable for cruising at high transonic Mach numbers. CFD analysis could be performed on the whole wing configuration however this must be used with caution as it comes at a larger cost, increased setup time and uncertainties associated with the accuracy of the mesh used. At this stage, wing thickness has likely been made too large to allow for fuel storage integration at an underestimated reduction of aerodynamic efficiency.

### 12.1.3 Folding Wing Tip

Initially, the weight of the folding wing tip was determined through a linear scaling of the wing size of the 777X to analyse structural calculations. Information about the mechanism was limited as it is a relatively new concept and consequently, values were estimated. This system is hard to design for and the complexity was underestimated at the beginning. More emphasis on how the system operates could have been done if time permitted. An additional role could have been created to look into this system in detail such as regulations and feasibility.

## 12.2 Way of Working & Team Management

The team structure was decided early on in the project to allow additional time for each group member to familiarise themselves with the deliverables for their role. After this, the project manager and chief engineer roles were assigned by a democratic vote. Due to the interconnected nature of the task, team roles were sometimes fluid, however, the project manager ensured work was split evenly and progress goals were met on time.

Communication between the group was carried out via several channels (Figure 18a): WhatsApp group messaging for informal communication, formal group updates through a Teams channel, task delegation and status observation on Monday.com, Overleaf to create collaborative documents for the

PEDR and FEDR, and PowerPoint to create collaborative presentations for the PDR and FDR. This method eliminated any unnecessary communication and facilitated harmonious and efficient teamwork within the group.

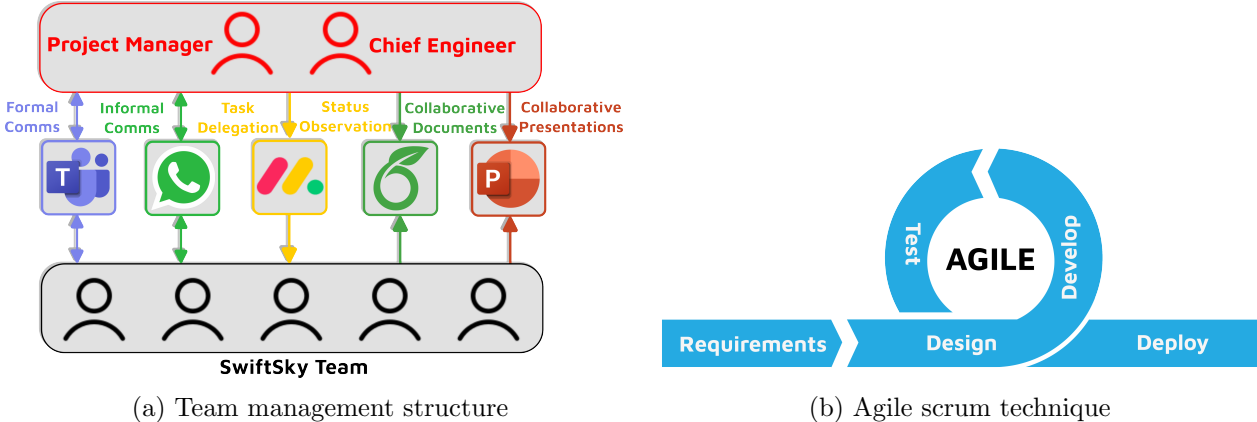


Figure 18: SwiftSky team way of working

Following the PEDR, the project was split into three sprints using the Scrum technique, a part of the Agile project management methodology - Figure 18b. Each sprint was its own design iteration, ending in a design freeze where the current configuration was reviewed by the whole group before the next sprint. Progress goals were regularly checked by reviewing the Gantt chart (which was made at the beginning of the project - Figure 48 in appendix) to ensure the team was on schedule.

### 13 CONCLUSION

In this report, the process of designing a 4200 *NM* range, 2-class 170-passenger aircraft is presented. The main objective was to design an aircraft that would occupy a market gap by reducing the aircraft's DOCs by 15% when compared to its competitors.

To achieve this, the team focused on several key factors: decreasing fuel consumption through high aerodynamic efficiency; increasing utilisation by reducing transit time and turnaround time; making the airframe lighter and more structurally efficient through optimal use of composite materials; and decreasing the manufacturing and maintenance costs. As a final design, the SwiftSky team has come up with a conventional configuration with the addition of a folding wing-tip mechanism to increase the wingspan while adhering to the 36 *m* gate limit.

Despite all other requirements and objectives being met, the DOC reduction of 15% was ultimately not achieved. A total DOC reduction of 6% was achieved, however, with further iteration, a larger reduction could have been reached.

The DOC reduction target was not reached due to several factors. The main reasons were identified as the engine operating outside of its design range and the EIS date making novel concepts unfeasible, so additional efficiency gains from new technologies could not be utilised.

Ultimately the design does have the potential to improve on the current market, but would not be worth pursuing for EIS 2030. Airlines are unlikely to replace their current fleet unless a DOC reduction of around 15% is reached. If the EIS was pushed back sufficiently, a larger DOC reduction could be achieved with the implementation of different engines and new technologies, allowing the SwiftSky aircraft to perform much better in the market.

## Part II

# Technical Description

## 14 SYSTEMS

### 14.1 Electrical Systems

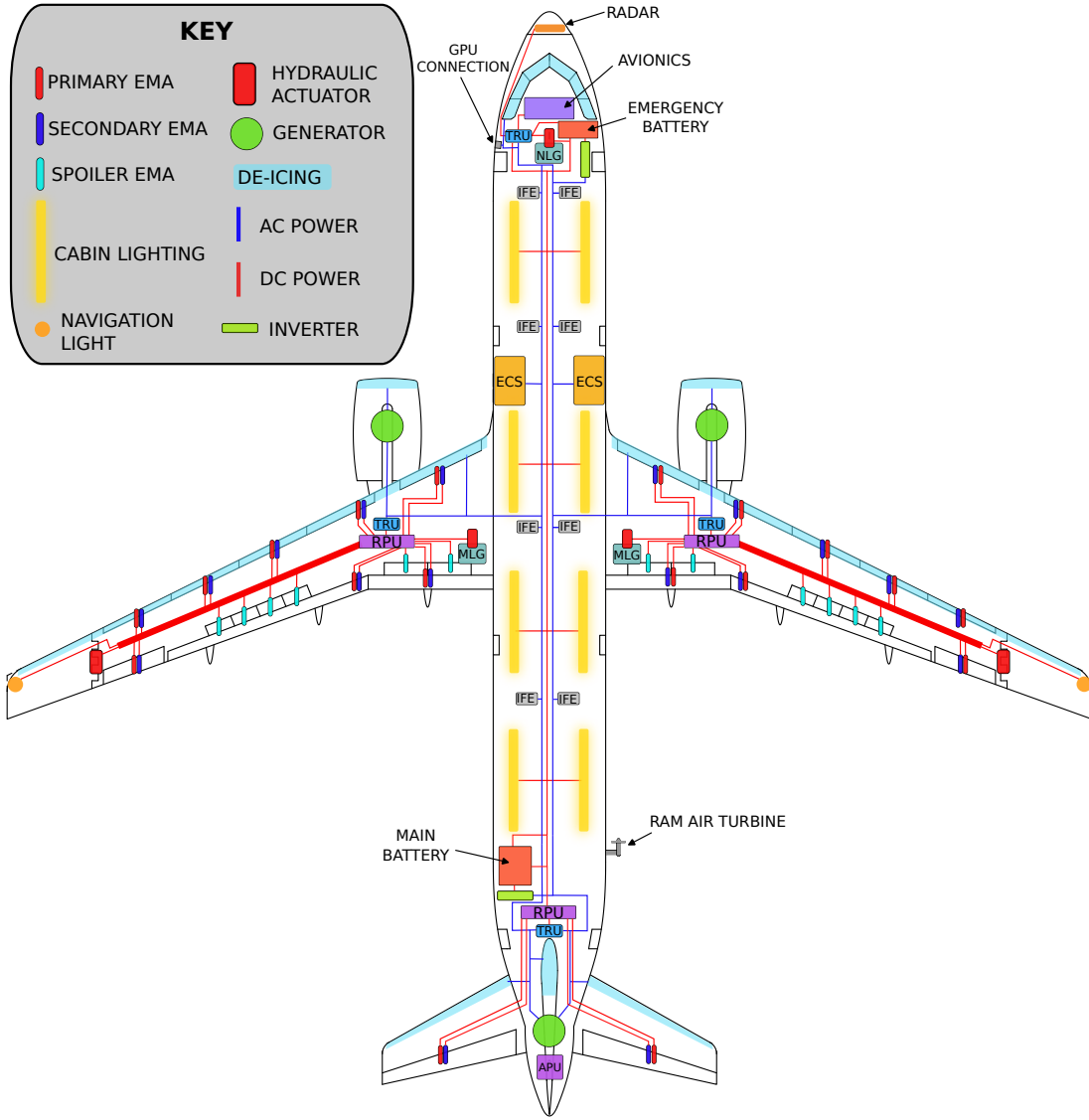


Figure 19: Electrical systems

Figure 19 shows the electrical systems architecture for the SwiftSky aircraft. A more electric architecture (MEA) was adopted to increase the engine efficiency. This reduces the need for hydraulic and pneumatic systems, significantly for engine bleed air in systems such as deicing and air conditioning, hence increasing thrust available, allowing for weight reduction and easier maintenance.

A  $250\text{ kVA}$  variable speed constant frequency (VSCF) generator is to be fitted on each engine and on the APU, scaled from the B787 [24] [25]. A  $28\text{ V}$  main battery is also to be included for secondary power supply, along with an emergency battery and RAT for emergency use. Current can be converted from each power source to AC or DC through inverters and transformer rectifier units (TRUs). Control surfaces are actuated by electro-mechanical actuators (EMAs), with secondary EMAs fitted on ailerons and high-lift devices for redundancy.

A consideration was initially made for a design with no APU, with the latter being replaced by a battery. The necessity for this secondary source of power is due to power supply for: engine startup, ECS operation in-ground, alternative electricity supply following in-flight engine failure. The use of a battery would result in significant weight saving due to the incorporated removal of the fire suppression systems required in the presence of an APU. Furthermore, in-ground power can be supplied by the ground power unit (GPU) which could make use of renewable energy generation as well as reducing fuel burn. However, due to the requirement to adhere to CAA ETOPS regulations, an APU had to be fitted given the SwiftSky aircraft design mission [26].

## 14.2 Avionics

The SwiftSky aircraft is to be fitted with avionics to satisfy CS-25 safety requirements, as well as ACARS II, “Enhanced“ Mode S and RVSM certification. The required components include:

- Auto-pilot & auto-land capabilities up to CAT IIIB weather conditions.
- Enhanced Mode S & ADS-B system for enhanced safety & efficiency.
- All-glass flight deck with EVS II system and HUDs to aid situational awareness during low visibility conditions.
- System health management
- Collision avoidance systems including TCAS & GPWS
- Flight recorders
- RNP-01 4D navigation system
- Temperature, speed and pressure sensors
- Inertial navigation system (INS)

## 14.3 Fuel Systems

The most important driver to sizing the fuel tanks was to hold 34930 L of the required mission fuel with reserves. Due to the main rib that holds the engine a three-tank concept built into the wing box was designed to reduce sloshing. The maximum fuel capacity is divided into various tanks in the aircraft as shown in Table 15. All the fuel tanks have cross-feed valves that feed every tank to the engine and separate the fuel in tanks so that leakage does not affect the other. The RCTs were aimed to be placed near the centre of the aircraft to prevent drastic changes in CoG during flight or rolling motion. Figure 20 shows the components of the fuel system. A dry bay will be positioned directly behind each engine to store the electrical equipment for each wing.

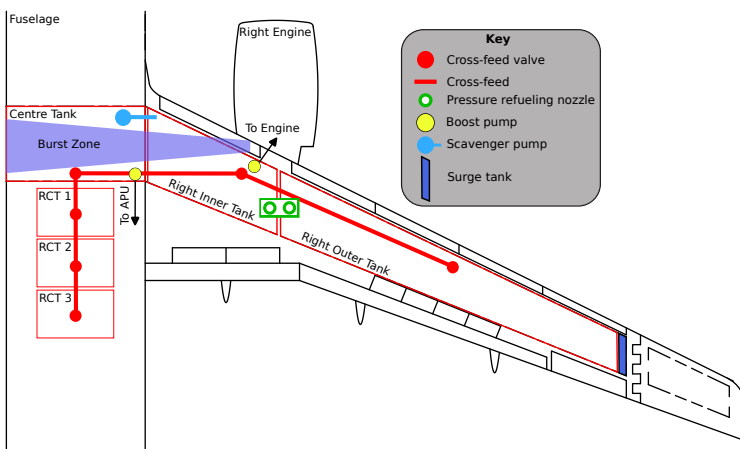


Figure 20: Fuel systems

Table 15: Maximum fuel capacity

Fuel Tanks	Volume [L]
Inner Tanks	11575
Outer Tanks	5965
Centre Tank	8871
RCTs x3	10500
Total	36911

## 14.4 Folding Wing Tip

An electro-hydraulic system shall be implemented for the wing tip hinge mechanism. To allow for easier certification the wingtip mechanism shall be designed to adhere to CS-25 regulations for control

surfaces. This required two independent locking systems for redundancy [13]. The actuation system shall be hydraulic actuation with a torque of  $8.5 \text{ kNm}$  that will only be operated on the ground to mitigate failure to deploy in flight and will hydro-lock in its extended position to prevent folding of the wingtips in flight. The locking system shall be an electrically actuated pin-locking system. The pin-locking system shall only disengage when electrically powered so that in the event of electronic failure the wing tip remains locked and extended. The pin shall be titanium to provide a high strength-to-weight ratio. The wing-tips will fold upwards so that ground clearance and access for emergency vehicles are not impeded. The LE will be de-iced in the same manner as other control surfaces.

## 15 WEIGHT, STABILITY & CONTROL

### 15.1 Weight Breakdown

The OWE of the aircraft was initially calculated using Sadraey's method [12] and the technical specification [1]. Weights for components such as the fuselage, wings, tailplane, fin, undercarriage, fixed equipment, and operational items were calculated. The propulsion system was sized with the TF30 engine, and the wing tip hinge mechanism was scaled to the relative span of the Boeing 777X's mechanism. Further design iterations and study refined the weights, resulting in OWE values of  $47451 \text{ kg}$  and  $47040 \text{ kg}$  for the 170 and 222 passenger variants, respectively.

The MTOW is  $98909 \text{ kg}$  as highlighted in Table 16. These weights were determined by analysing fuel load fractions required for the  $4200 \text{ NM}$  hard design requirement and using the AVDASI-3 tools consisting of payload-range diagrams, block fuel and block time plots for finding optimal cruise speeds and altitudes. The payload, including passengers, crew, and baggage (with each passenger weighing  $105 \text{ kg}$ ), contributes to increased fuel requirements for the mission, resulting in a significant difference in MTOW between the two configurations.

Table 16: Design weights of low-density and high-density configurations

Design Weights [kg]	222 variant	170 variant
MWE	39,770	39,770
OWE	47,040	47,451
MZFW	70,424	66,946
MRW	99,123	90,989
MLW	84,072	77,158
<b>MTOW</b>	<b>98,909</b>	<b>90,775</b>

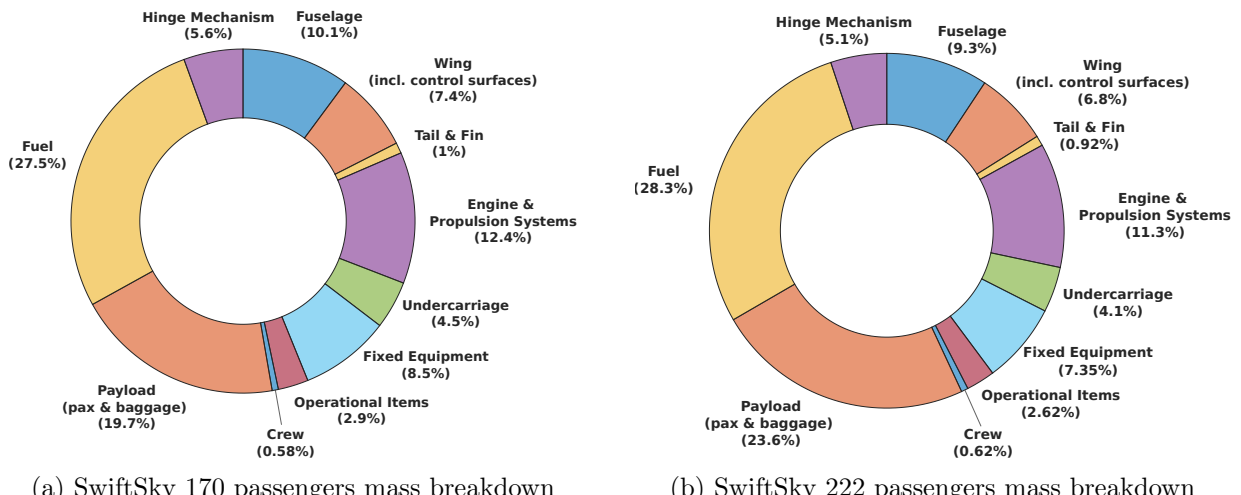


Figure 21: SwiftSky mass breakdowns

The mass breakdown of SwiftSky, detailing component weights for low and high-density designs, is

presented below in Figure 21. Initial calculations utilised the Jenkinson method [27], considering comparable aircraft like the A321XLR and B757-200. In-depth analysis, encompassing material choices, engine sizing, wing area, landing gear studies and systems integration ensured precise mass breakdown predictions as percentages.

## 15.2 CoG calculations

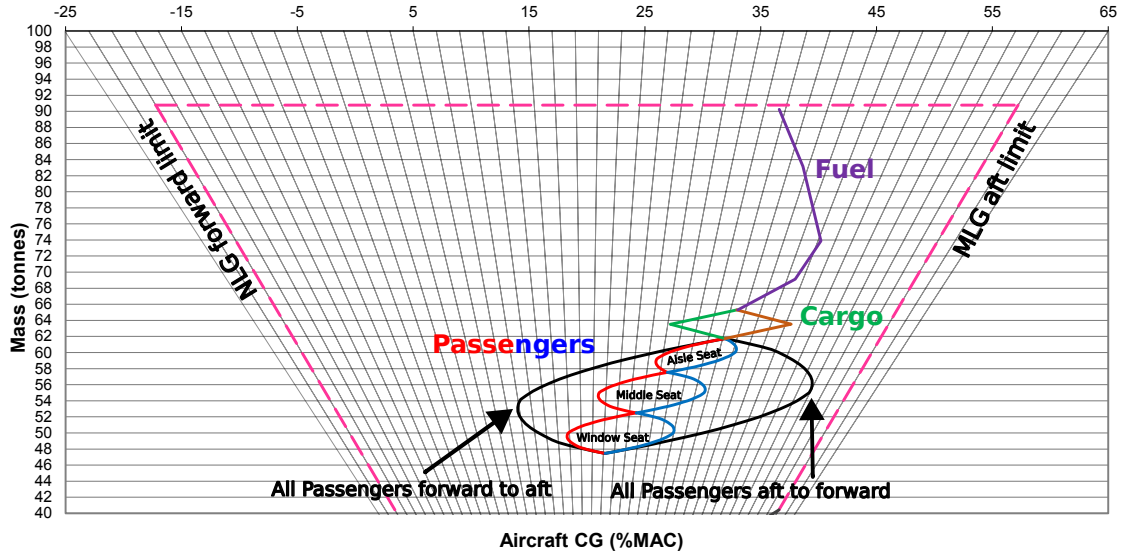


Figure 22: SwiftSky 170 passengers extreme loading cases

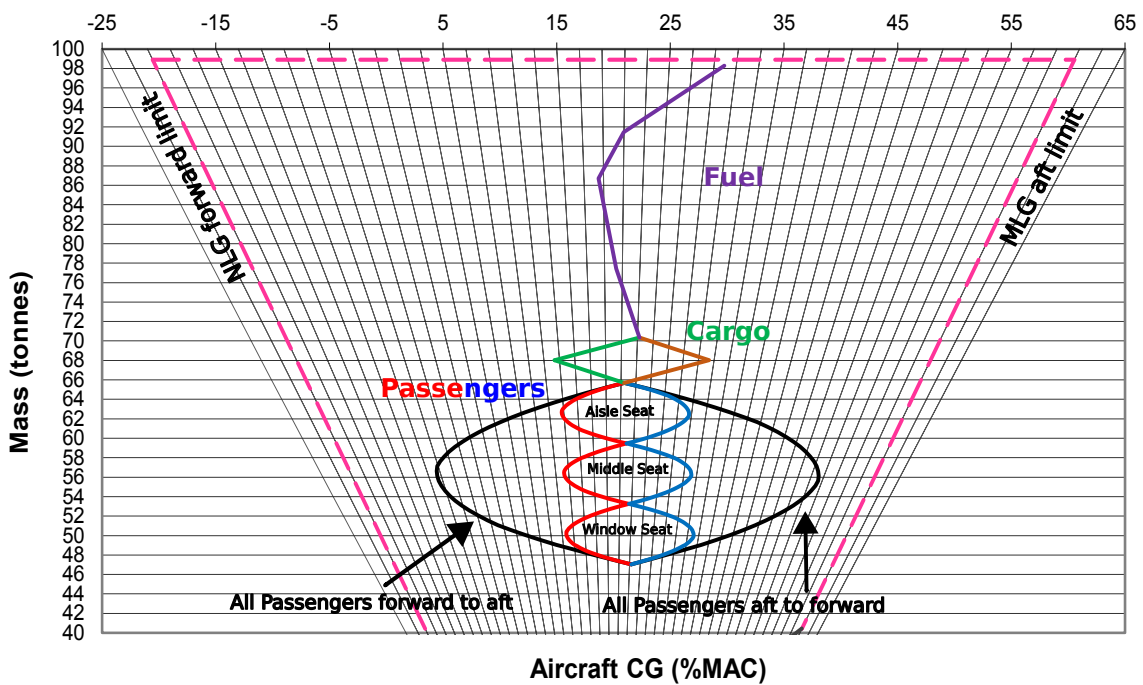


Figure 23: SwiftSky 222 passengers extreme loading cases

The OWE CoG for both configurations is situated at 23.3% MAC. Extreme load cases were assessed, with the most forward take-off and landing CoG determined by the NLG structural limit due to buckling constraints (see Figure 22). The critical loading case, involving no fuel, no rear cargo, and passengers loading from forward to aft, satisfies limits.

The maximum allowable aft CoG for take-off and landing is dictated by the MLG structural limit after which the tail strike follows due to failure of NLG adherence. The furthest aft CoG arises from no fuel, passengers loading from aft to forward, and rear cargo hold loaded.

In the extreme loading cases graphs below the high-density 222-passenger configuration shows a takeoff CoG of 29% MAC [23], while the low-density 170-passenger configuration has a take-off CoG of 38% MAC [22].

### 15.3 Stability & Control

The empennage and control surfaces were initially sized using tail volume coefficients and span fractions from Sadraey [12] and then verified and iterated using MIT's AVL to ensure requirements were met. A summary of the key points follows:

1. **Neutral Point:** Found to be at 62.8% MAC. Behind CoG to ensure static stability, allowing the aircraft to return to steady flight after perturbation.
2. **Take-off and landing performance:** A pitch rate of  $3.32 \text{ }^{\circ}/\text{s}^2$  was achieved during takeoff complying with the requirement for a pitch rate between  $3 - 5 \text{ }^{\circ}/\text{s}^2$  [12].
3. **Aircraft trim:** Tail area and setting angle enable effective aircraft trim across all flight conditions within the specified CoG range.
4. **Roll rate:** Ailerons sized according to CS 25.147, ensuring the aircraft rolls from  $-30^{\circ}$  to  $+30^{\circ}$  in under 7 seconds with the aircraft capable of performing this manoeuvre in 5.9 seconds at the trimmed cruise condition.
5. **Asymmetric thrust for OEI:** Tail sized to meet yawing moment to counteract asymmetric thrust during an engine failure [13].
6. **Crosswinds:** Rudder design exceeds CS 25.237 specifications, allowing for a maximum cross-wind landing of  $27 \text{ kts}$ , outperforming the maximum required of  $25 \text{ kts}$  [13].
7. **Longitudinal stability:** The tail sizing has been verified to be longitudinally stable with a pitching moment/angle of attack ( $\frac{\partial C_M}{\partial \alpha}$ ) value of  $-5.52$  for the trimmed cruise condition.

## 16 STRUCTURES & MANUFACTURING

### 16.1 Wing Structures

The wing box is designed with two spars, ribs and skin stiffened with stringers, which is a typical wing structural design [28]. For the structural calculations, the wing box was modelled as a hollow cantilever beam with a varying rectangular cross-section. The width was chosen to be 55% of the chord (Figure 9), after considering the size of the HLD listed in Table 19 and leaving the required space for their actuation mechanisms. The wing box height reduces linearly from 18% of the chord at the root to 10% of the chord at the tip. The wing box is split into two sections (Figure 8) due to the folding wing hinge and mechanism. The second section in the folding wing tip is necessary as it is  $3.3 \text{ m}$  long and therefore needs to withstand  $118 \text{ kNm}$  of bending moments at the hinge as shown in Figure 26. However, the gap between the two wing box sections, shown in Figure 8, was not considered in the model for simplicity, it was assumed the entire wing contains a continuous wing box, which means the skin thickness in that small region will be underestimated. Extra skin thickness will be needed to make up for the lack of spars in that gap. The wing box in the folded wing tip does not store any fuel, reducing its weight and bending moment at the hinge. However, the sweep and

dihedral angles of the wing were not considered in this model due to time constraints, which means the model underestimates the torque experienced by the wing box.

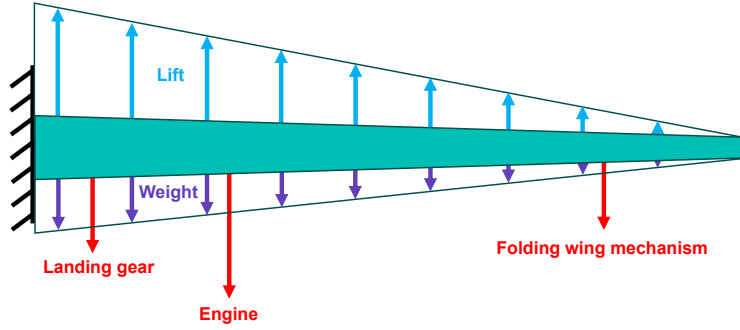


Figure 24: Free body diagram of wing box

The lift and wing weight (wing structure and fuel) were assumed to have a triangular distribution, with the highest load at the root (Figure 24). Engine, landing gear and folding wing mechanism weights were modelled as point loads. The triangular distribution for the lift was chosen because the taper ratio of the wing was chosen to be below the optimum value to increase load distribution towards the root, making the lift distribution less elliptical. For the wing weight, triangular distribution was used because the wing is the thickest and widest at the root and linearly gets slender up to the tip. The fuel storage is also linked to the dimensions of the wing, so more fuel is stored near the root. The total lift force of the aircraft was calculated to be  $1305\text{ kN}$  by taking moments about the main wing AC, and the load from the MTOW at the CoG along with a lift force at the horizontal tail AC were considered. The initial estimate of the wing structural weight was calculated using Sadraey's method [12], which was then revised to be  $3923\text{ kg}$  after wing box sizing iterations using the method outlined by Ajaj et al. [29]. The folding wing mechanism weight was estimated to be  $2528\text{ kg}$  by scaling down the Boeing 777X's folding mechanism weight [30] by comparing the folding wing tip spans of the Boeing 777X and SwiftSky aircraft. For torque calculations in the chordwise direction, the folding wing mechanism CoG was assumed to be at the centre of the wing box, the wing weight was estimated to be acting at 39.9% of the chord, the engine CoG and landing gear position was calculated to be  $1.56\text{ m}$  ahead of the LE and  $4.05\text{ m}$  behind the LE respectively, based on their mounting positions.

Even though the shear force, bending moment and torque diagrams (Figures 25, 26 and 27) show all three load cases ( $1g$ ,  $2.5g$  and  $-1g$ ), only the most extreme case of  $2.5g$  was used for all design decisions along with an ultimate safety factor of 1.5 [14] to ensure the structure can withstand all types of loads without catastrophic failure. Additionally, a material knockdown factor of 1.14 [15] was used to account for environmental factors such as changes in temperatures during flight and fatigue cycles.

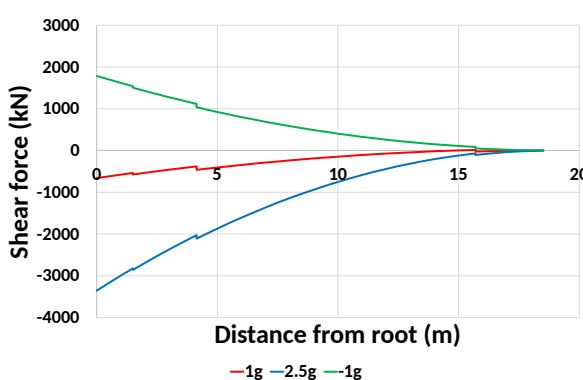


Figure 25: Shear force diagram

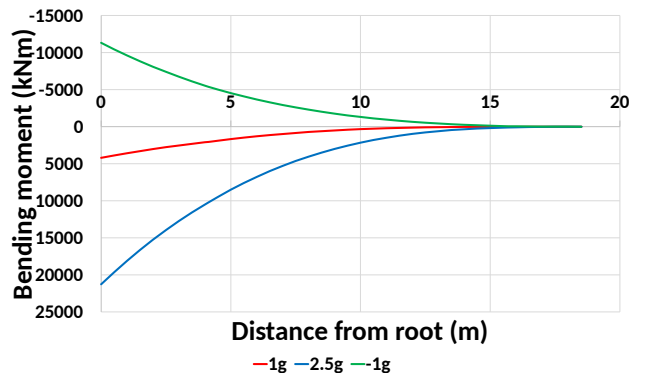


Figure 26: Bending moment diagram

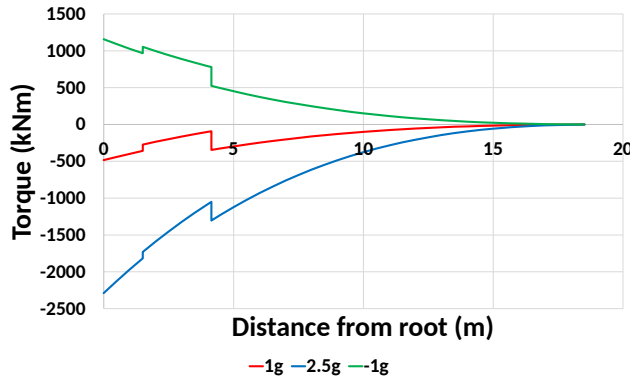


Figure 27: Torque diagram

The thickness of both spars is designed to be equal and it is assumed they resist the vertical shear forces and torsional loads. Similarly, the thickness of both upper and lower skin panels is equal and they resist bending and torsional loads. The method outlined by Ajaj et al. [29] was used to calculate the required thickness of the spars and skins, which varies along the span as shown in Figures 3 and 4. Note the increase in thickness where the engine is fixed to withstand the increased load. This varying thickness design was preferred over constant thickness designs for it is structurally more efficient. The gap in the spar thickness diagram highlights that there is no spar there due to the folding hinge mechanism, however, the skin panels still exist there. The thicknesses are a multiple of 0.184 mm, which is the ply thickness of Hexcel IMA/M21 pre-impregnated (prepreg) CFRP [31]. It was assumed that the cured ply thickness of a resin-infused carbon fibre fabric is going to be similar to that of prepregs (usually around 0.125 mm [32]), so the numbers of plies for the spar and skin are listed in Table 27 of Appendix. Both thickness values are high compared to that of the A350 [33] [34], even though this aircraft is a lot smaller. However, this seems reasonable because the SwiftSky aircraft contains a very heavy folding wing hinge mechanism very far outboard, which produces very large bending moments, unlike the A350 which does not have a folding wing tip.

The wing box design consists of 26 ribs per wing perpendicular to the LE (Figure 8) for structural efficiency and it is more conventional [28]. The rib pitch is 686 mm, which is calculated with the method from Torenbeek [35] to ensure the upper skin panel does not column buckle under compressive loads. The spacing is constant to reduce manufacturing costs. From the calculations, it was possible to have larger rib spacings which would reduce weight, but it was chosen to be 686 mm to ensure the engine is mounted on a rib (6th rib in this design). Even though the rib pitch is higher than that of the A320 (calculated using [36] [37]), it is acceptable because of the relatively thick skins which reduce buckling.

The stringer spacing (Figure 8 and 9) is calculated using the flat plate buckling theory from Megson [38] to ensure the upper skin between the stringers does not buckle with compressive loads. The number of stringers needed in one skin panel is 20, with the spacing between them reducing along the span from 119.0 mm at the root to 48.8 mm at the tip. With larger spacing between the stringers, weight is saved as fewer stringers are needed, but this reduces the critical buckling stress, so an optimum solution is found where the critical buckling stress is maximised while minimising weight. The number of stringers was kept constant to make the design simple and reduce manufacturing costs. Hat-stringers were chosen because they allow the structural weight to be low with fewer materials and manufacturing costs compared to other types such as the J-stringers [39].

## 16.2 Material Selection

The main wing (except LE skin), HTP, VTP (except LE) and engine nacelles are all manufactured out of CFRP (Figure 28). CFRP is lightweight while being very stiff and strong [40], allowing it to reduce the weight of the aircraft, directly increasing their fuel efficiency. The nose cone is made of AFRP and LE of the VTP is made of GFRP (Figure 28) because both composite materials are radio-transparent. Additionally, AFRP has good impact-resistant properties making it suitable for the nose cone, as bird

strikes are more likely to happen with it. These composites are also cheaper than CFRP. The layup for all the composite sections starts with a ply of copper mesh for lightning strike protection [41], as the composite materials used are non-conductive.

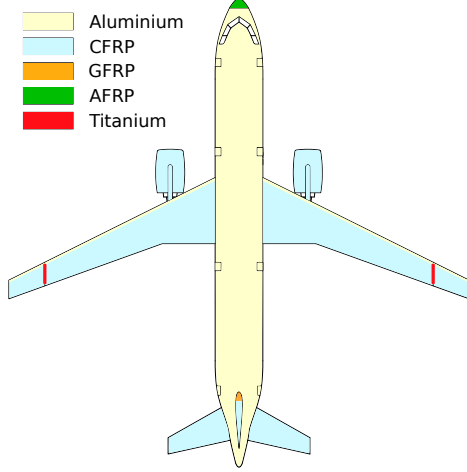


Figure 28: Material usage breakdown

Aluminium is used for the fuselage (Figure 28) of the aircraft because of its high strength and low density, which means the structure will be light. It will also be cheap to manufacture with aluminium as the technology is very mature for this application. The aluminium alloy AA2524-T3 can be used for the fuselage structures as it has excellent damage tolerance [42]. Even though composites would make the structure lighter, the material and manufacturing cost is higher than with metals, so the weight saving might not be justified, as the weight efficiency of mid-range aircraft is not as important as that of long-range aircraft. If composites were used for the fuselage, delamination could happen which is difficult to inspect, increasing the DOC. For the same reason of reducing DOC, the LE skin of the main wing is made of aluminium, as it is a flow-facing component and is more likely to have impacts.

Titanium is used to make the folding wing hinge because of its very high strength and high corrosion-resistant characteristics. It also has a better strength-to-weight ratio than steel [43], which is necessary for this critical component while minimising weight.

Overall, 50% of the aircraft structural weight is constituted by composite materials as shown in the material usage percentage breakdown chart in Figure 12. This can be achieved by 2030 with the current state of composite technology as current long-range aircraft (Airbus A350 and Boeing 787) already contain about 50% composites [44] and the similarly sized new aircraft Irkut MC-21 contains 40% composites by weight [45]. The older Airbus A320 has 28% composite by airframe weight [46] and compared to that, SwiftSky can achieve a lower DOC because of reduced weight from increased composite usage makes the aircraft more fuel efficient. A trade study (Figure 29) was conducted to evaluate the RDTE and manufacturing costs with varying composite usage. A value of 50% was chosen as a result of this study as it gave the best balance between low RDTE and manufacturing costs.

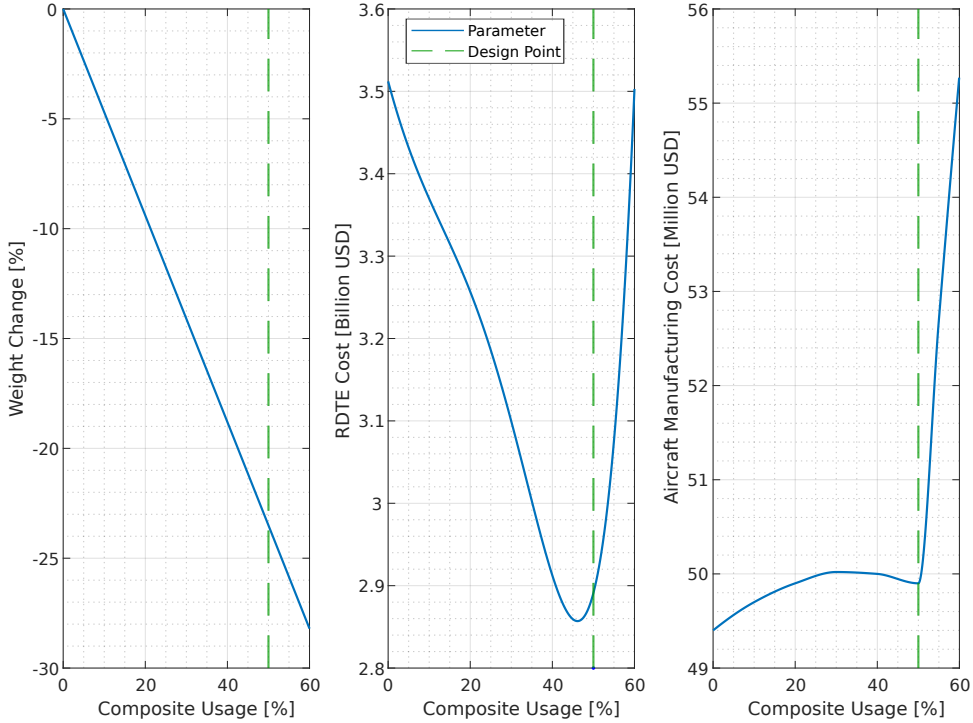


Figure 29: Material trade-off study

### 16.3 Manufacturing

For composites manufacturing, Resin Transfer Infusion (RTI) will be used where dry stacked plies of non-crimp fabric (NCF) are vacuum bagged with the mould and then resin is fed into the plies. This process is a lot cheaper than using prepgres which are more traditionally used [41]. RTI is the latest composite technology adapted in aircraft manufacturing by the Airbus A220 programme [47], so its certification is achievable as it has been proven to work. Achieving high fibre volume fraction (FVF) is more difficult with the RTI technology, however, with careful manufacturing processes, the FVF can be close to that of traditional tape-laid prepgre structures, and the porosity in the part can also be made very low [41].

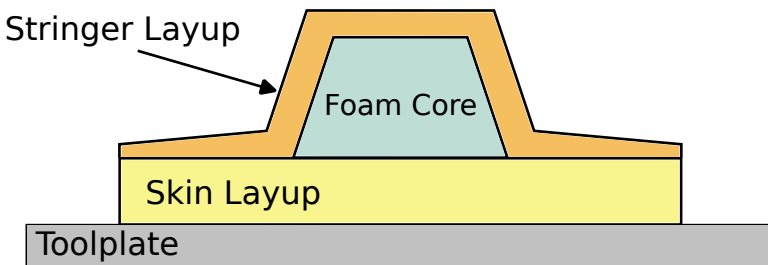


Figure 30: Skin-stringer infusion with high-density closed cell foam core

To eliminate the need to bond the stringers onto the skin, a method has been proposed to infuse the stringers together with the skin in one single process (Figure 30). After the plies for the skin are stacked on the mould, a high-density closed-cell foam core is placed, on top of which further plies are stacked to form the stringers. After this, the entire setup is vacuum-bagged and infused with resin. The high-density foam core does not add any significant weight to the structure while reducing steps in manufacturing, and reducing cost. The foam core needs to be closed cell so that if there is a leakage, the foam does not absorb any fuel and becomes dead weight. Certification of this new development will be difficult, but critically following the design approval process highlighted by the UKCAA [48]

can help prove the concept to be safe for aerospace applications. The aluminium stringers and frames in the aluminium fuselage are attached using traditional methods such as fasteners, which keep the manufacturing and research costs low.

## 17 AERODYNAMICS

### 17.1 Wing Design

Wing area was initially sized using a constraint diagram, Figure 31, from Sadraey [12], the design point selected was chosen to accommodate constraint variations during the design iterations and to reduce required thrust-to-weight. The optimal aspect ratio for reducing DOC was determined from Figure 7. Root chord and kink size were sized from Sadraey [12] to allow sufficient room for landing gear integration. An optimisation on wing aerodynamic efficiency with twist and taper ratio is shown in Figure 32, with a compromise taper ratio of 0.28 selected. A taper ratio below the aerodynamic optimum increased loading distribution towards the root, mitigating wing bending moments. However, reducing the taper ratio too much was constrained by the risk of the wing tip chord being too small for integrating a hinge mechanism. The twist is set at  $-2^\circ$  at the tip, driven by the need for the root to stall first to maintain control authority in the event of stall. The span-wise distribution of the final wing in isolation is shown in Figure 33, please note that the fuselage has not been modelled so values from  $-2.2\text{ m}$  and  $2.2\text{ m}$  must be considered with caution.

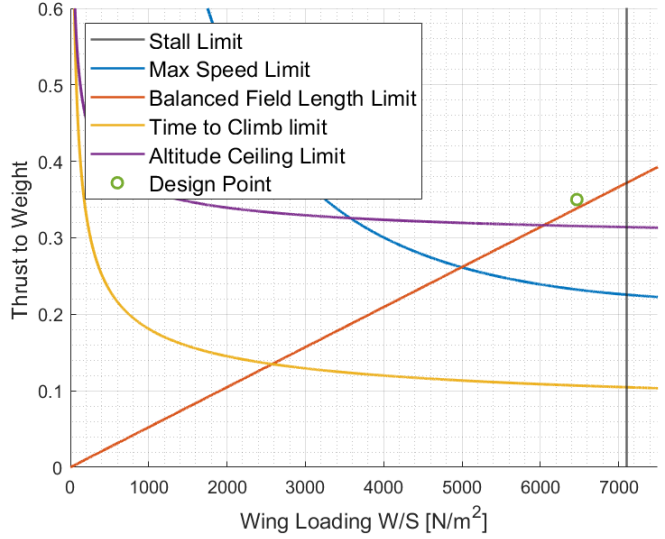


Figure 31: Constraint diagram

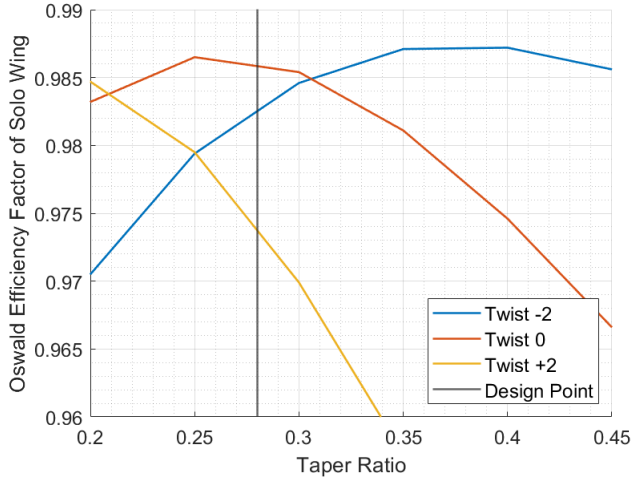


Figure 32: Taper and twist against span-wise efficiency

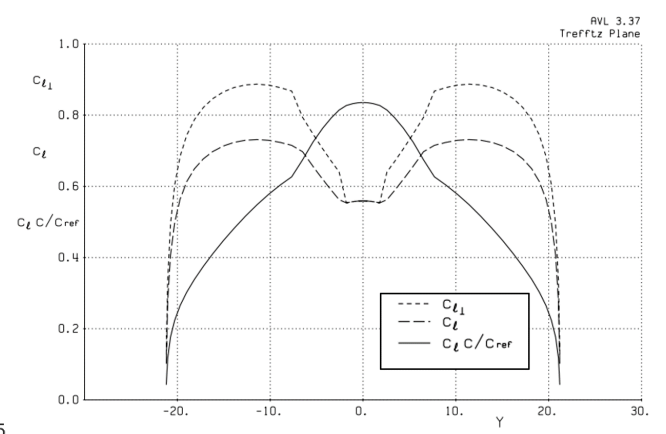


Figure 33: Span-wise lift distribution for the wing in isolation

### 17.2 Aerofoil & Cruise Performance

The required cruise lift coefficient ( $C_L$ ) was determined to be 0.581 at Mach 0.82, calculated based on average cruise mass, altitude, and density. Using approximations from Sadraey [12] and Raymer [49]

the required  $C_L$  for the aerofoil section was found to be 0.611. Considering the transonic cruise speed a NASA Phase 2 supercritical aerofoil family was chosen specifically the NASA SC(2)-06XX series due to its design lift coefficient of 0.6 [10] the aerofoils utilised are shown in Table 17. A different aerofoil family is employed for the root location due to limited data on the design lift coefficient. The chosen thickness variation of the aerofoil sections along the span minimises required RCTs and drag, maximising fuel storage efficiency in the wing. See Table 18 for configuration details.

ESDU's VGK 2-D CFD software [50] was used to identify the drag rise with the Mach number for the root aerofoil section. Figure 34 and the Boeing definition for drag divergence [49] identified  $M_{DD} = 0.77$ . Using ESDU 78009 [51] the wing was swept to  $23.7^\circ$  so that drag divergence for the aircraft occurs at  $M = 0.84$ ; above the cruise Mach number.

Table 17: Aerofoils

Aerofoil	Location	Thickness, t/c [%]
SC(2)-0610	Tip	10
SC(2)-0614	Kink	14
SC(2)-0518	Root	18

Table 18: RCT and  $C_D$  with wing thickness

Root/Kink/Tip t/c [%]	RCTs	$C_{D_{Wing}}$
<b>18/14/10</b>	3	0.001934
18/14/12	3	0.001950
14/14/12	4	0.001866
14/14/10	4	0.001854
14/12/10	4	0.001830

The drag buildup described in section 17.4 was used with MIT's AVL software to provide lift and drag coefficients at the cruise configuration. Figure 35 shows the L/D polar where  $L/D_{Cruise} = 20.05$ . This surpasses the 17 of the 757-200 [22] and the 19 of the A321 [23], emphasising our design's superior aerodynamic efficiency compared to main competitors.

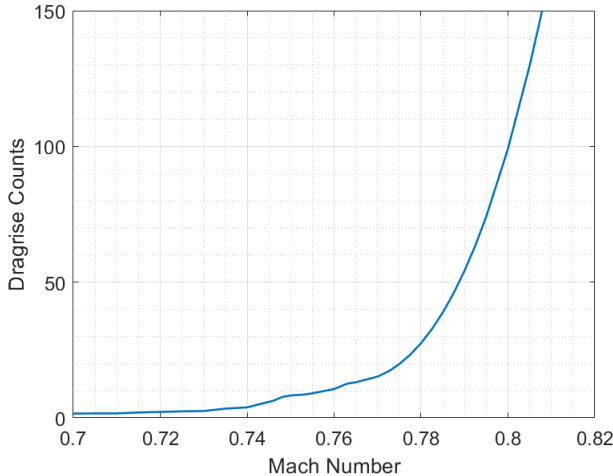


Figure 34: Drag rise counts against Mach number for the root aerofoil section

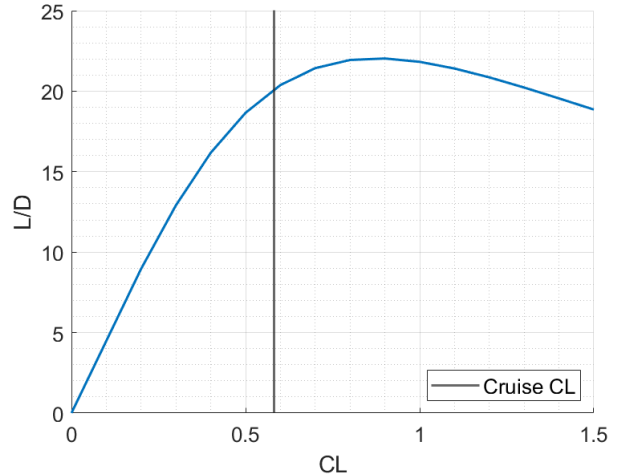


Figure 35: L/D polar for aircraft in cruise configuration

### 17.3 High Lift Design

The HLD configuration includes a LE Slat and a TE double-slotted flap, detailed in Table 19 with  $\delta$  representing deflection from the horizontal chord line. Lift curve slopes for different configurations are presented in Figure 36, derived using ESDU LiCrA toolbox [52]. From Figure 36 it can be observed that the HLD increases the maximum lift coefficient at all angles of attack at the compromise of a reduced stall angle. The  $C_{LMax}$  is constrained by the tail strike angle during landing and take-off, resulting in  $C_{LMax} = 2.91$  at landing and  $C_{LMax} = 2.82$  at take-off. The need for significant HLD deflection and chord sizes arises from the reduced percentage of span available as beyond the wingtip hinge no lifting devices are present. The large deflections do come at the cost of increased drag which was predicted by methods outlined by Raymer [49] and is presented in the polar in Figure 38.

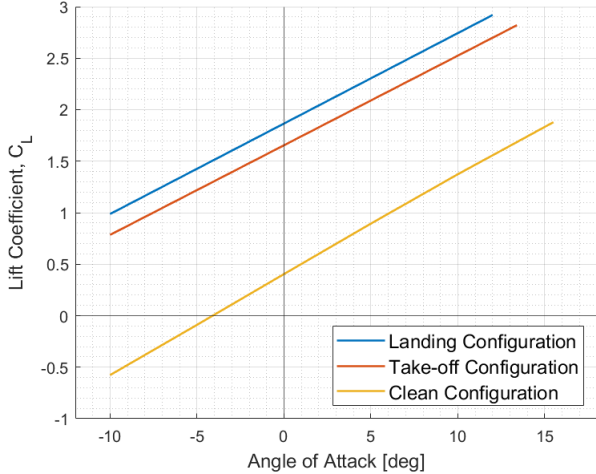


Figure 36: Lift curve slopes for whole aircraft  
(clean at approach conditions)

## 17.4 Drag

The aircraft's  $C_{D0}$  is determined as 0.01859 using Raymer's empirical drag buildup method [49], illustrated in Figure 37. This method involves component-wise analysis, considering the wetted area, laminar flow percentage, form factor, and interference factor. A conservative approach was used which assumes low laminar flow percentages as a worst-case scenario: 5% over the fuselage, 10% over the wings, and none over the nacelles. This approach results in the fuselage being the dominant source of drag. Leakage and protuberance are assumed at 5% [49]. Transonic operation requires the addition of a wave drag component, approximated using Lock's first-order equation [11]. Miscellaneous drags account for upsweep and flow separation from rearward-facing flat areas. Given the first-order nature of Lock's equation, future development may benefit from a more refined drag buildup utilising CFD analysis.

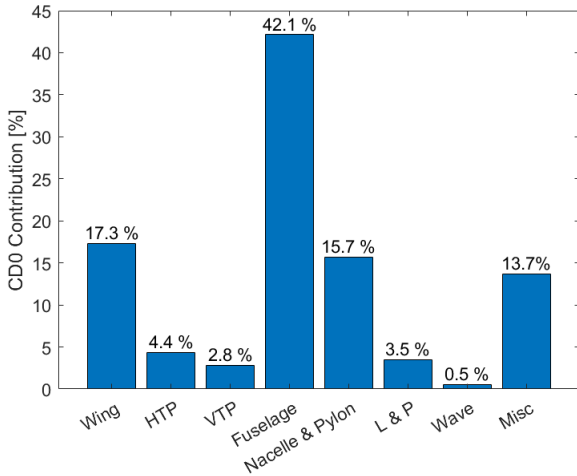


Figure 37:  $C_{D0}$  build-up for aircraft in cruise configuration

Table 19: HLD Configuration

	Slat	Flap 1	Flap 2
Chord Fraction [%]	10	10	15
Span Fraction [%]	75	60	60
Take-off $\delta$ [°]	25	10	35
Land $\delta$ [°]	30	15	45

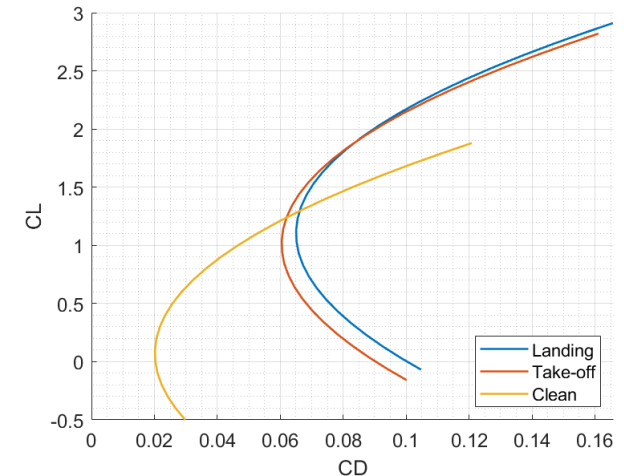


Figure 38: Drag polar for whole aircraft

## 18 LANDING GEAR

### 18.1 Configuration and Integration

A conventional retractable tricycle landing gear configuration was chosen as it provides excellent stability during take-off and landing, better visibility from the flight deck, and ease of loading and unloading cargo and passengers as the aircraft is level on the ground which results in lower turnaround times. The MLG retracts towards the fuselage centreline under the wing behind the wingbox due to its wide wheeltrack. Retraction under the fuselage was not possible due to the lack of underfloor cargo space. The NLG retracts forward into the underfloor of the cabin of the fuselage. The MLG has two legs with two tyres each and the NLG has one leg with two tyres each to satisfy the one flat tyre requirement. The gear doors and retraction systems are operated hydraulically. In case of nose gear collapse, sufficient ground clearance reduces engine damage.

### 18.2 Design Philosophy

The runway limits were obtained from ICAO Code 4C and summarised in Table 20 [53]. The main objectives were to size the landing gear for future family extensions for up to a 15% increase in MTOW and to reduce the ACN as this would damage the runways less and incur less maintenance and landing fees. Positioning the landing gear along the fuselage was iterated many times as it varies with CoG positions. All the weights and respective CoG positions were considered as the MLG had to be placed aft of the most aft position of the CoG of the aircraft to maintain ground stability and prevent tipping. Static and dynamic load analysis for three major load cases (CS 25.493, CS 25.495, CS 25.491) were done to confirm the chosen dimensions and consequently used for sizing the other components. Integration was important as this was limited to the space available behind the wingbox with the necessary clearance.

Table 20: Runway Limits

ICAO Code 4C	
Wheel track	< 9.0 m
Turnover angle	< 63 deg
Turn width	< 24.0 m
Runway Code X	
Tyre Pressure	< 217.6 psi

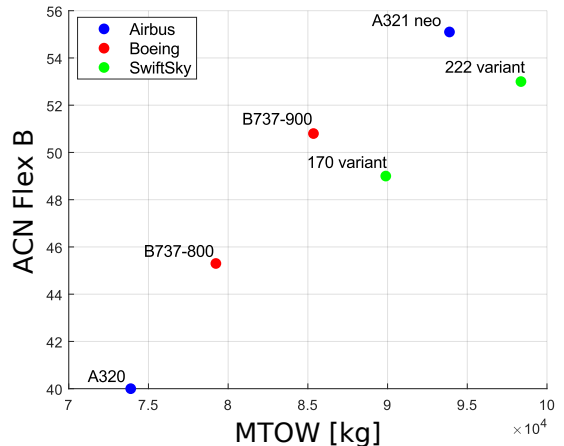


Figure 39: ACN compared to competitors.

### 18.3 Final Design

The positioning of the MLG was placed at 21.00 m from the nose and this is 0.8 m aft of the worst CoG position the aircraft can endure and near the strut attachment point. The NLG was placed 6.30 m as the wheelbase and wheel track had to be sized iteratively to satisfy the limits of the turnover angle and turn width. As a result, the max load share the NLG can take at the most forward position was 20.41% and at the most aft position the load share of the MLG was 94.56%. This was within the range of the steering capacity of the nosewheel steering system. Due to this specific configuration, the ACN calculated was 52.7 which was very competitive among similar aircraft as shown in Figure 39. The final dimensions are summarised in Table 21.

Table 21: Final landing gear dimensions

Parameters	Value	Units	Parameters	Value	Units
Nose to NLG	6.30	m	ACN	52.7	-
Nose to MLG	21.00	m	Steering angle	75.0	°
Wheelbase	14.70	m	MLG load @ MTOW	92.50	%
Wheel track	7.40	m	NLG load @ MTOW	7.50	%
Turnover angle	58.89	°	Tail-Strike angle	12.0	°
Turn width	23.61	m	Ground clearance	0.61	m

## 18.4 Tyre Sizing

Radial and bias tyres were compared and radial was chosen as they weigh and wear less which reduces ACN [54]. For tyre sizing, the 15% increase in MTOW, a safety factor of 7%, and a single tyre operating load while braking with the highest possible load share were used as these simulate the most extreme conditions that the landing gear can endure. Tyres were compared from various manufacturers such as Goodyear [55], Michelin [56], and Dunlop [57]. The rated load on the tyre had to withstand the worst possible case and due to the limits of Code X runway, the tire pressure is limited to  $217.6\text{ psi}$  [58]. All these considerations showed that the ideal tyre size for the MLG was 52x20.5R20 and NLG was 30x11.5R14.5 with respective tire pressures of  $211.23\text{ psi}$  and  $103.99\text{ psi}$  which are below the limit. The ACN obtained for this configuration was 52.7 with a 92.5% load on MLG at MTOW which is lower than the A321neo with a MTOW of  $94\text{ tonnes}$ . This was calculated with the COMFAA 3.0 software [59] and was compared with similar aircraft as shown in Figure 39.

## 18.5 Brake Sizing

Carbon brakes were chosen as they provide a 35% weight reduction compared to steel brakes, however, they are three times the width as they have 6 stators and rotors compared to steel brakes with 2 stators and rotors. This was justified as carbon brakes last longer and have improved energy absorption despite a high initial cost. The carbon brakes have a rim size of  $20"$  with a width of  $353\text{ mm}$ . Only the MLG has braking compatibility as this prevents the aircraft from tipping backwards due to the nose-down pitching moment. Each wheel has one brake pack on the MLG. Brake sizing was driven by the rejected take-off case and this was found by calculating the kinetic energy of the aircraft the brakes absorb during landing at a 5% increase in the landing speed of  $140\text{ kn}$ . Thrust reversers and spoiler use were not accounted for during the braking calculations to have a safety margin.

## 18.6 Shock Absorber and Material Analysis

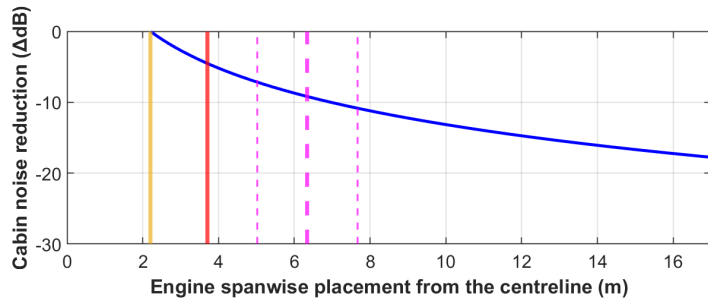
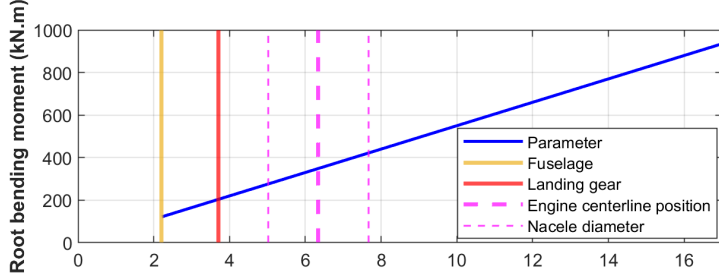
Oleo-pneumatic shock absorber was used with a stroke length of  $499\text{ mm}$  and a piston diameter of  $231\text{ mm}$ . When the absorber is unloaded the pressure was designed to be  $281.8\text{ psi}$  while at the bottoming load, it was  $5008\text{ psi}$ . Simple load and buckling analysis was done between Aluminium 7075, Steel alloy 300M, and titanium alloy Ti-6Al-4V. The aluminium alloy cannot withstand the required buckling loads and membrane stresses and was immediately disregarded. To further justify material selection, an analysis between the weight and cost was studied. Titanium alloy costs 8 times more than steel alloy for the same weight [21]. As a result, the strut and the brace assemblies were made from Ti-6Al-4V due to its high strength-to-weight ratio. The shock absorber piston and other linkages are made from steel as they reduce the overall cost of the landing gear to around \$650,000. Two analytical methods from Currey were used to estimate the mass of the landing gear initially but the bottom-up method gave a more accurate value of  $4845\text{ kg}$  which is 5.8% of the MLW [60].

## 19 PROPULSION & PERFORMANCE

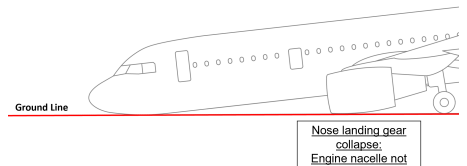
### 19.1 Engine Scaling

The engine thrust was dictated by the aircraft's ability to meet the take-off field length requirement in the OEI condition at airfield elevations up to 5000 ft (Figure 42). This led to an engine thrust scaling of 1.18.

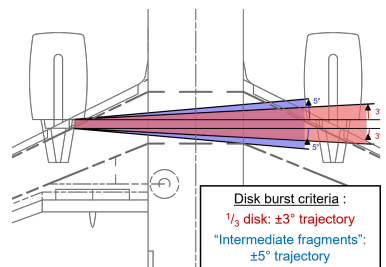
### 19.2 Engine Position



(a) Engine spanwise placement constraints



(b) Nose landing gear collapse scenario



(c) Turbine disk burst scenario

Figure 40: Engine placement constraints

After the engine was scaled, its exact position needed to be determined. To select the spanwise placement, a trade-off study between minimising the  $-1g$  bending moment at the root, by bringing it inwards and reducing the cabin noise, by moving the engine outwards. Thus, a distance of 6.34 m from the fuselage centerline was considered satisfactory for both situations, without interfering with the landing gear (Figure 40a).

For the engine's chordwise positioning, two failure scenarios were taken into account. The first one was the nose landing gear collapse, in which case the engine would not risk hitting the ground (Figure 40b). The second one was that in the case of a turbine disk burst, for which it is assumed that 1/3 of any disk travelling radially has infinite energy [61]. Thus, the engine has to be positioned such that in the event of a disk burst, the rear spars of both wings are outside the direct trajectory ( $\pm 3^\circ$ ) and intermediate trajectory ( $\pm 5^\circ$ ) of the debris (Figure 40c). Both these constraints were satisfied by placing the engine 14.34 m away from the aircraft nose (distance taken from the inlet cowl lip).

### 19.3 Take-off and Landing

Figure 42 shows the runway distances required for normal take-off, aborted take-off and the most critical scenario, the OEI case. The critical power failure speed  $V_1$  was found by determining the balanced field length (Figure 41). Knowing this distance is crucial for the pilot to determine whether to continue the take-off in case of an engine failure [27]. Once  $V_1 = 69.7 \text{ m/s}$  was determined and the take-off speed was assumed to be 1.2 times greater than the stall speed at MTOW ( $V_{stall} = 68.9 \text{ m/s}$ ) [62], the take-off distance was computed over a range of different airfield elevations (Figure 42).

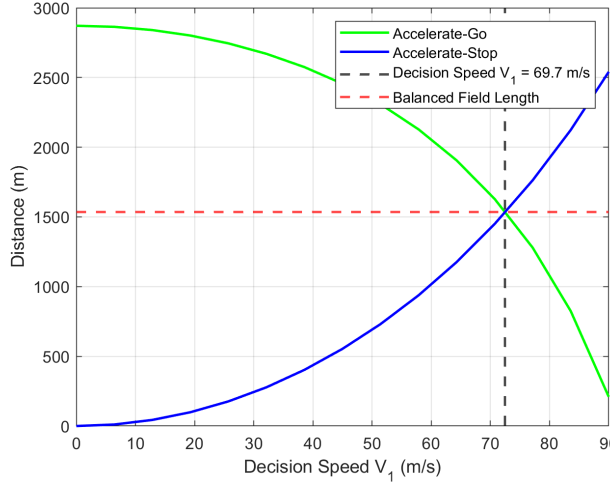


Figure 41: Balanced field and decision speed at SLS ISA+15

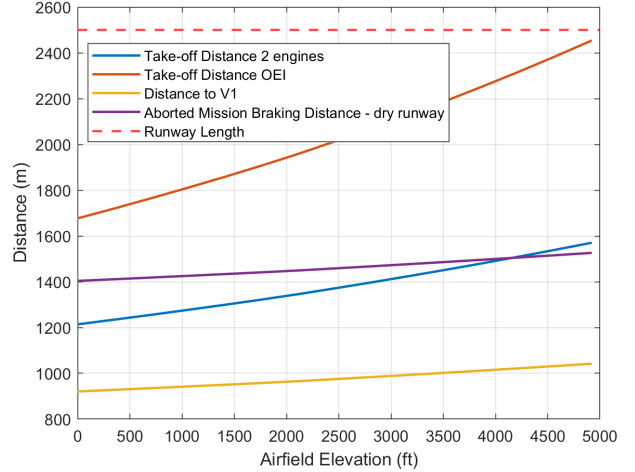


Figure 42: Take-off field length increase with airfield Elevation

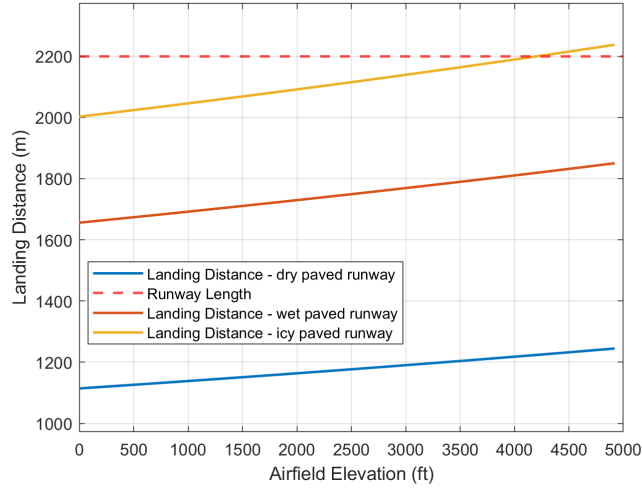


Figure 43: Landing field length increase with airfield elevation

For the landing performance, three scenarios were studied (Figure 43). For all of them, the touch-down speed  $V_{TD}$  was assumed to be equal to the reference speed ( $V_{ref} = 1.3V_{stall}$ ) [63] without applying any corrections related to wind and weather conditions. The first case was the dry landing, for which the braking friction coefficient was  $\mu = 0.5$  and the wheel friction coefficient of 0.02. The second case was landing on a wet paved runway, with the braking friction coefficient of  $\mu = 0.3$ . In the case of landing on an icy runway, the braking friction coefficient considered was  $\mu = 0.1$ . All values for friction coefficients are the maximum allowable values, as per Jenkinson *et al.* [27]. The landing distances for all these cases needed to be factored by 1.66 to account for uncertainties during landing, according to the JAR/FAR certification rules [27].

For both the dry landing and wet landing cases, the aircraft complies with the requirement of landing distance  $\leq 2200\text{ m}$  across all airfield elevations considered. Landing on an icy runway at high elevations, however, would not meet the requirement. A solution would be the use of reverse thrust while braking in this situation.

## 19.4 Cruise Performance

The initial cruise altitude was limited by the rate of climb (*RoC*) at the top of climb  $\geq 300 \text{ ft/min}$  requirement. The *RoC* at 35,000 ft was found to be 349  $\text{ft/min}$ , which is why it was selected as the initial cruise altitude.

Cruising is performed using the stepped climb technique in steps of 2000  $\text{ft}$ , from the initial cruise altitude to the final one of 41,000  $\text{ft}$ . Since the performance tool was unable to model step climb, several assumptions needed to be made to represent each step. For ease of calculation, the intermediate climb phases were assumed negligible and for each step, the amount of fuel that the aircraft needed to burn to be able to climb to the next altitude with a  $\text{RoC} \geq 300 \text{ ft/min}$  was calculated. For the first step, 50% of the total fuel of 16237 kg burned in cruise, 30% for the second, and 15% for the third, leaving the rest of 5% to be used at the final cruise altitude. A breakdown of the mission phases can be found in the appendix in Table 26. For more accurate results, a tool capable of accounting for step climb needs to be developed.

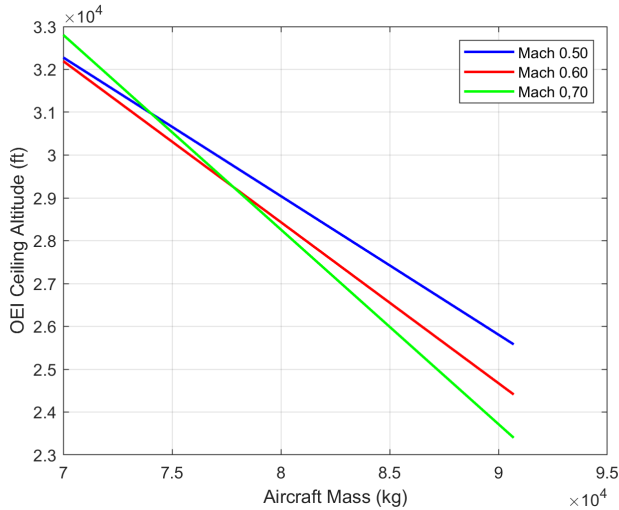
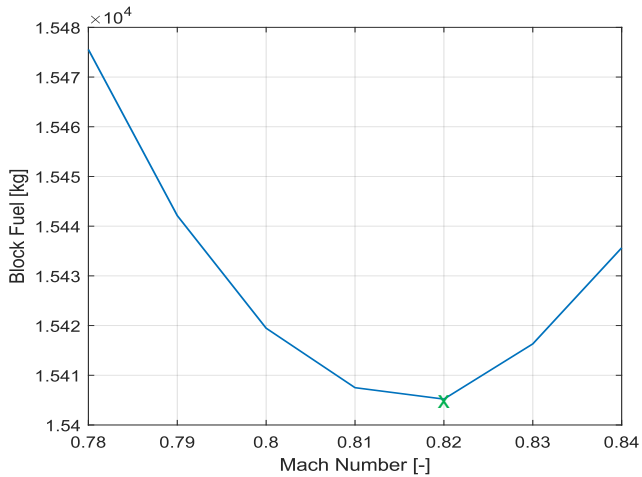


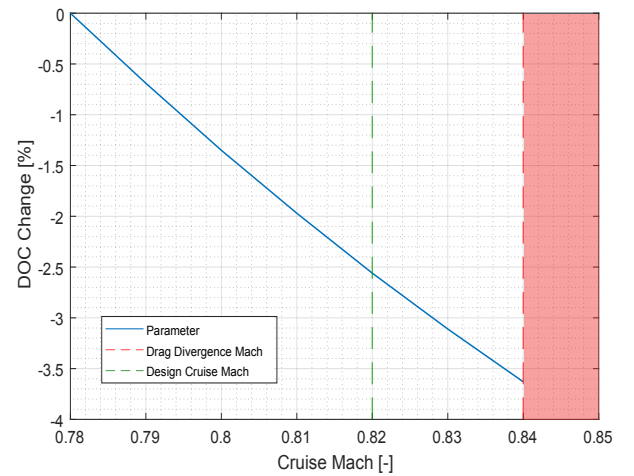
Figure 44: Altitude ceiling - one engine failure during cruise

In the event of an engine failure during cruise, the altitude that the aircraft can cruise at has been computed in Figure 44, based on the amount of fuel that it has already burned. The OEI cruise ceiling also depends on the reduction in Mach number.

The cruise Mach number was selected based on the lowest block fuel output for the study mission, Mach number 0.82 (Figure 45a). Although the DOC decreases with the increase in Mach number (Figure 45b), the Mach number 0.82 is more robust with the fuel price fluctuations.



(a) Study mission block fuel used while cruising at different Mach numbers



(b) Change in DOC with the increase of cruise Mach number

Figure 45: Mach number selection study

## 19.5 Noise

Using the methods highlighted in ICAO Annex 16 [64], noise pollution levels were calculated and found to be within the ICAO limits - Table 22.

Table 22: Noise pollution levels

	<b>ICAO limit</b>	<b>Achieved</b>
Lateral full-power noise level (EPNdB)	119.34	95.6
Approach noise level (EPNdB)	120.97	118.39
Flyover noise level (EPNdB)	126.57	109.64

## REFERENCES

- [1] Keith Macgregor. Student design project specification. Airbus Future Projects, 2023.
- [2] FlyZero. Market forecasts and strategy. <https://www.ati.org.uk/wp-content/uploads/2022/03/FZ0-CST-REP-0043-Market-Forecasts-and-Strategy.pdf>, 2022. Accessed 23rd November 2023.
- [3] Aviation Week. Airbus launches long-range a321neo version. <https://aviationweek.com/air-transport/airbus-launches-long-range-a321neo-version>. Accessed 25th October 2023.
- [4] Flight Global. A321lr first single-aisle to beat 757-300 economics. <https://www.flightglobal.com/fleets/arkia-chief-a321lr-first-single-aisle-to-beat-757-300-economics/130272.article>. Accessed 25th October 2023.
- [5] Airbus. A321xlr - the single-aisle xtra long range route opener. <https://aircraft.airbus.com/en/aircraft/a320/a321xlr>. Accessed 25th October 2023.
- [6] Airbus. Global market forecast 2023-2042. <https://www.airbus.com/en/products-services/commercial-aircraft/market/global-market-forecast>, 2023. Accessed 23rd November 2023.
- [7] Boeing. Boeing forecasts demand for 42,600 new commercial jets over next 20 years. <https://investors.boeing.com/investors/news/press-release-details/2023/Boeing-Forecasts-Demand-for-42600-New-Commercial-Jets-Over-Next-20-Years/default.aspx>, 2023. Accessed 23rd November 2023.
- [8] Airbus. Orders and deliveries commercial aircraft. <https://www.airbus.com/en/products-services/commercial-aircraft/market/orders-and-deliveries>, 2023. Accessed 23rd November 2023.
- [9] Boeing. Orders and deliveries. <https://www.boeing.com/commercial/#/orders-deliveries>, 2023. Accessed 1st December 2023.
- [10] Charles D Harris. Nasa supercritical airfoils: A matrix of family-related airfoils. Technical report, 1990.
- [11] Christopher Noel Hunter Lock. The ideal drag due to a shock wave. parts i and ii. 1945.
- [12] Mohammad H Sadraey. *Aircraft design: A systems engineering approach*. John Wiley & Sons, 2012.
- [13] EASA. Easa cs-25 european aviation safety agency certification specification for large aeroplanes, 2003.
- [14] T.H.G. Megson. Chapter 13 - airworthiness. In T.H.G. Megson, editor, *Aircraft Structures for Engineering Students (Seventh Edition)*, Aerospace Engineering, pages 449–454. Butterworth-Heinemann, seventh edition edition, 2022.
- [15] Han-Pin Kan. Assessment of probabilistic certification methodology for composite structures. Technical report, Office of Aviation Research, US Federal Aviation Administration, 2001.
- [16] University of Bristol. Additional notes - estimation of direct operating costs – AEA method, 2013. Accessed 23rd November 2023.
- [17] J. Roskam and University of Kansas. *Airplane Design: Part 8 - Airplane Cost Estimation: Design, Development, Manufacturing and Operating*. DARcorporation, 1985.
- [18] FlightGlobal. Airbus outlines expected market impact of A320neo. <https://www.flightglobal.com/airbus-outlines-expected-market-impact-of-a320neo/97220.article>, 2010. Accessed 27th November 2023.

- [19] Florian Jaehn and Simone Neumann. Airplane boarding. *European Journal of Operational Research*, pages 339–359, 2015.
- [20] European Commission. European commission decision C (2014)4995 of 22 july 2014. [https://ec.europa.eu/research/participants/portal4/doc/call/h2020/common/1617621-part\\_19\\_general\\_annexes\\_v.2.0\\_en.pdf](https://ec.europa.eu/research/participants/portal4/doc/call/h2020/common/1617621-part_19_general_annexes_v.2.0_en.pdf), 2020. Accessed 3rd December 2023.
- [21] Global Market Insights. Aerospace landing gear market size worth over \$19 bn by 2026. <https://www.gminsights.com/pressrelease/aerospace-landing-gear-market>, 2020. Accessed 11th November 2023.
- [22] Boeing. 757 passenger and specification. [https://www.boeing.com/resources/boeingdotcom/company/about\\_bca/startup/pdf/historical/757\\_passenger.pdf](https://www.boeing.com/resources/boeingdotcom/company/about_bca/startup/pdf/historical/757_passenger.pdf), 2007. Accessed 23rd October 2023.
- [23] Airbus. A321 aircraft characteristics, airport and maintenance planning. <https://skybrary.aero/sites/default/files/bookshelf/2370.pdf>, 2005. Accessed 23rd October 2023.
- [24] Vincenzo Madonna, Paolo Giangrande, and Michael Galea. Electrical power generation in aircraft: Review, challenges, and opportunities. *IEEE Transactions on Transportation Electrification*, 4(3):646–659, 2018.
- [25] Boeing. 787 propulsion system. [https://www.boeing.com/commercial/aeromagazine/articles/2012\\_q3/pdfs/AERO\\_2012q3\\_article2.pdf](https://www.boeing.com/commercial/aeromagazine/articles/2012_q3/pdfs/AERO_2012q3_article2.pdf).
- [26] UK Civil Aviation Authority. Cap 513 extended range twin operations (etops). <https://publicapps.caa.co.uk/docs/33/CAP513.pdf>.
- [27] Lloyd R Jenkinson, Paul Simpkin, Darren Rhodes, Lloyd R Jenkinson, and Rolls Royce. *Civil jet aircraft design*, volume 338. Arnold London, 1999.
- [28] MCY Niu. Airframe structural design: Practical design information and data mcy niu second edition. distributed by adaso/adastra engineering center, po box 3552, granada hills, ca 91394, usa, 1999. 612pp. illustrated. \$65. isbn 962-7128-09-0. *The Aeronautical Journal*, 105(1050):459–459, 2001.
- [29] RM Ajaj, MI Friswell, D Smith, and AT Isikveren. A conceptual wing-box weight estimation model for transport aircraft. *The Aeronautical Journal*, 117(1191):533–551, 2013.
- [30] SeekingAlpha. Boeing 777x: Every kilogram matters. <https://seekingalpha.com/article/4071222-boeing-777x-every-kilogram-matters>, 2023. Accessed 24th November 2023.
- [31] Hexcel. Hexply m21. [https://hexcel.com/user\\_area/content\\_media/raw/HexPly\\_M21\\_global\\_DataSheet.pdf](https://hexcel.com/user_area/content_media/raw/HexPly_M21_global_DataSheet.pdf), 2023. Accessed 4th November 2023.
- [32] Melih Papila. Design of and with thin-ply non-crimp fabric as building blocks for composites. *Science and Engineering of Composite Materials*, 25(3):501–516, 2018.
- [33] CompositesWorld. Update: Lower wing skin, wing of tomorrow. <https://www.compositesworld.com/articles/update-lower-wing-skin-wing-of-tomorrow>.
- [34] CompositesWorld. A350 a400m wing spars: A study in contrasts. <https://www.compositesworld.com/articles/a350-a400m-wing-spars-a-study-in-contrasts>, 2013.
- [35] Egbert Torenbeek. Development and application of a comprehensive, design-sensitive weight prediction method for wing structures of transport category aircraft. *Delft University of Technology, Faculty of Aerospace Engineering, Report LR-693*, 1992.
- [36] AviationHunt Team. Airbus a320 ata 06 (technical notes). <https://www.aviationhunt.com/airbus-a320-ata-06/>.

- [37] Airbus. Airbus a320 aircraft characteristics airport and maintenance planning. [https://aircraft.airbus.com/sites/g/files/jlccta126/files/2023-02/Airbus-techdata-AC\\_A320\\_0322.pdf](https://aircraft.airbus.com/sites/g/files/jlccta126/files/2023-02/Airbus-techdata-AC_A320_0322.pdf).
- [38] T.H.G. Megson. Chapter 9 - thin plates. In T.H.G. Megson, editor, *Aircraft Structures for Engineering Students (Seventh Edition)*, Aerospace Engineering, pages 331–367. Butterworth-Heinemann, seventh edition edition, 2022.
- [39] United States Patent 7871040. Composite aircraft structures with hat stiffeners. <https://www.freepatentsonline.com/7871040.html>.
- [40] Jens Sjölander, P Hallander, and Malin Åkermo. Forming induced wrinkling of composite laminates: A numerical study on wrinkling mechanisms. *Composites Part A: applied science and manufacturing*, 81:41–51, 2016.
- [41] CompositesWorld. Plant tour: Spirit aerosystems, belfast, northern ireland, u.k. <https://www.compositesworld.com/articles/plant-tour-spirit-aerosystems-belfast-northern-ireland-uk>.
- [42] Fernanda Martins Queiroz, Maysa Terada, Aline F Santos Bugarin, Hercílio Gomes de Melo, and Isolda Costa. Comparison of corrosion resistance of the aa2524-t3 and the aa2024-t3. *Metals*, 11(6):980, 2021.
- [43] Metal Supermarkets. Titanium vs steel: What is the difference? <https://www.metalsupermarkets.co.uk/titanium-vs-steel-what-is-the-difference/#:~:text=Strength%2Dto%2Dweight%20ratio%3A,superior%20corrosion%20resistance%20stands%20out>.
- [44] CH Lee, Mohd Sapuan Salit, MR Hassan, et al. A review of the flammability factors of kenaf and allied fibre reinforced polymer composites. *Advances in Materials Science and Engineering*, 2014, 2014.
- [45] Flightline Weekly. First flight of an mc-21-300 airliner with russia made composite wings. <https://www.flightlineweekly.com/post/first-flight-of-an-mc-21-300-airliner-with-russian-made-composite-wings#:~:text=%E2%80%9CThe%20share%20of%20composites%20in,unattainable%20for%20a%20metal%20wing>.
- [46] Adam Quilter. Composites in aerospace applications. <https://www.aviationpros.com/engines-components/aircraft-airframe-accessories/article/10386441/composites-in-aerospace-applications>.
- [47] DierkRaabe. Saertex extends carbon-fibre contract with bombardier. <https://www.composites.media/saertex-extends-carbon-fibre-contract-with-bombardier/>.
- [48] UK Civil Aviation Authority. Innovation hub guide for innovators: On the path to certification an introduction to initial airworthiness. [http://publicapps.caa.co.uk/docs/33/Initial%20Airworthiness%20Guide%20for%20Innovators%20\(CAP2289\)%20V3.pdf](http://publicapps.caa.co.uk/docs/33/Initial%20Airworthiness%20Guide%20for%20Innovators%20(CAP2289)%20V3.pdf).
- [49] Daniel Raymer. *Aircraft design: A conceptual approach*. American Institute of Aeronautics and Astronautics, 2012.
- [50] ESDU. Vgk method for two-dimensional aerofoil sections. *ESDU 96028*, 2004.
- [51] ESDU. A framework relating the drag-rise characteristics of a finite wing/body combination to the those of its basic aerofoil. *ESDU 78009*, 1978.
- [52] ESDU. Esdu licra: 3d lift curve aerodynamics for wings and wing/body combinations. *ESDU 92031*, 2003.

- [53] International Civil Aviation Organization. Icao abbreviations and codes. <https://www.icao.int/nacc/documents/meetings/2014/ecaraim/ref03-icaocodes.pdf>, 2010. Accessed 9th October 2023.
- [54] Aviation Hunt. Aircraft radial vs bias tyre. <https://www.aviationhunt.com/aircraft-radial-vs-bias-tyre/>, 2023. Accessed 1st November 2023.
- [55] Goodyear Aviation. The aircraft tire databook. <https://www.goodyearaviation.com/resources/tiredatabook.html>, 2023. Accessed 2nd November 2023.
- [56] Michelin Aircraft. Michelin tyre catalogue. <https://aircraft.michelin.com/documents>, 2022. Accessed 2nd November 2023.
- [57] Dunlop Aircraft Tyres. Tires for boeing 737 next generation (ng). <https://www.dunlopaircrafttyres.co.uk/aircraft/boeing-737-next-generation-tires/>. Accessed 2nd November 2023.
- [58] SKYbrary. Pavement classification number (pcn). <https://skybrary.aero/articles/pavement-classification-number-pcn>, 2023. Accessed 2nd November 2023.
- [59] Federal Aviation Adminstration. Comfaa 3.0 software. <https://www.airporttech.tc.faa.gov/Products/Airport-Safety-Papers-Publications/Airport-Safety-Detail/ArtMID/3682/ArticleID/10/COMFAA-30>, 2014. Accessed 2nd October 2023.
- [60] Norman S Currey. *Aircraft landing gear design : principles and practices*. American Institute of Aeronautics and Astronautics, 1988.
- [61] C Easa. Certification specifications for large aeroplanes, cs 25, 2009.
- [62] Virginia Tech Department. Vehicle performance notes on take-off and landing. <https://archive.aoe.vt.edu/lutze/AOE3104/takeoff&landing.pdf>, 2005. Accessed 1st November 2023.
- [63] SKYbrary. Unstabilised approach: Landing distance and final speed calculations. <https://www.skybrary.aero/tutorials/unstabilised-approach-landing-distance-and-final-speed-calculations>, 2023. Accessed 2nd November 2023.
- [64] Troy A Rolf. International aircraft noise certification. *J. Air L. & Com.*, 65:383, 1999.

## APPENDIX

### Trade-off Studies

Table 23: Wing Placement Trade Study

Criteria	Weight (1-5)	Low Wing	Mid Wing	High Wing
Maintenance Access	4	3	2	1
Weight	3	3	1	2
Ease of Loading	4	2	1	3
Aerodynamic Efficiency	5	2	3	1
Landing gear integration	3	3	2	1
Ground Clearance	5	1	2	3
Cost	2	3	1	3
<b>TOTAL</b>		<b>59</b>	48	51

Table 24: Engine Placement Trade Study

Criteria	Weight (1-5)	Above Wing	Below Wing	Rear Fus.
Weight	4	1	3	2
Structural Stability	3	1	3	2
Structural Complexity	4	1	3	2
Aerodynamic Efficiency	5	2	1	3
Ground Clearance	5	2	1	3
Maintenance Access	5	2	3	1
Safety	3	1	3	1
Debris Ingestion	2	2	1	3
<b>TOTAL</b>		48	<b>69</b>	66

Table 25: Empennage Trade Study

Criteria	Weight (1-5)	Conventional	T-Tail	V-Tail	H-Tail	Cruciform
Weight	3	0	-2	+1	-2	-1
Structural Complexity	4	0	-1	-2	-2	-2
Maintenance Access	5	0	-1	-1	-1	0
Stability	2	0	-1	-2	+1	-1
Aerodynamic Efficiency	5	0	+2	+1	+1	0
<b>TOTAL</b>		<b>0</b>	-7	-9	-12	-13

## Turnaround Times

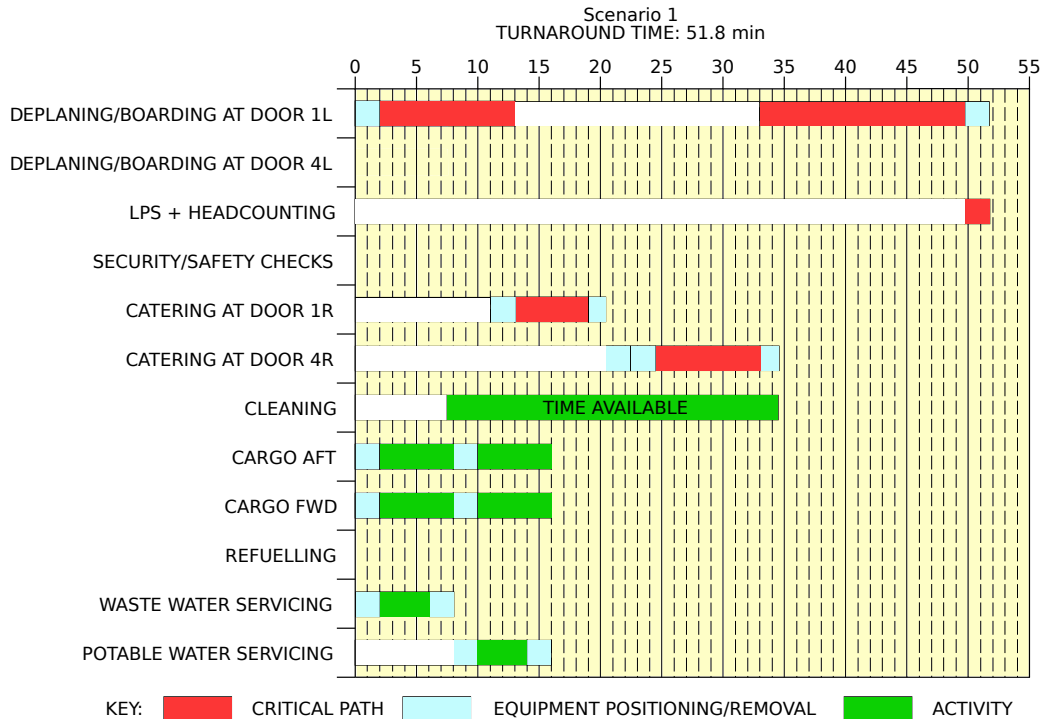


Figure 46: Turnaround Times for Scenario 1

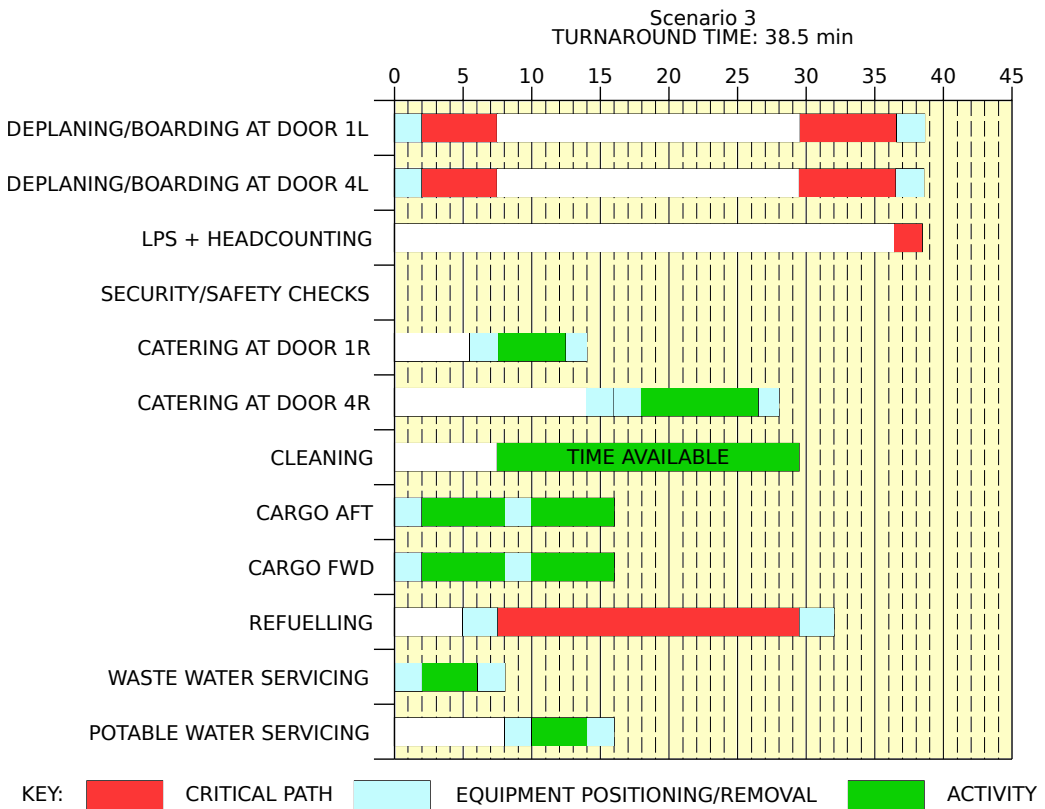


Figure 47: Turnaround Times for Scenario 3

## Turnaround Time Assumptions

### 1. PASSENGER HANDLING

222pax (1-class layout).

All passengers deboard and board aircraft.

2 stairs used at door 1L and 4L.

Equipment positioning and opening door = +2 min.

Closing door and equipment removal = +1.5 min.

No Person of Reduced Mobility (PRM) on board.

Deplaning:

- 111 pax at door 1L.
- 111 pax at door 4L.
- Deplaning rate = 20pax/min per door.

Boarding:

- 111 pax at door 1L.
- 111 pax at door 1L.
- Boarding rate = 13.2 pax/min per door.
- LPS + head counting = +2 min.

### 2. CARGO

2 cargo loaders.

Opening door + equipment = +2 min.

Equipment removal + closing door = +1.5 min.

100% cargo exchange:

- FWD cargo compartment: 4 containers.
- AFT cargo compartment: 4 containers.
- Bulk compartment: N/A.

Container unloading/loading times:

- Unloading = 1.5 min/container.
- Loading = 1.5 min/container.

### 3. REFUELING

25,000 L at 50 psig. No optional coupling. (22 mins).

Dispenser positioning/removal + connection/disconnection times = +2.5 min.

Refuelling with passengers on board: No.

### 4. CLEANING

Cleaning performed in available time.

### 5. CATERING

1 catering truck for servicing galleys sequentially at doors 1R and 4R.

Equipment positioning + opening door = +2 min.

Closing door + equipment removal = +1.5min.

Time to drive from one door to other = +2 min.

Full Size Trolley Equivalent (FSTE) to unload and load: 12 FSTE

- 5 FSTE at door 1R
- 7 FSTE at door 4R

Time for trolley exchange = 1.2 min per FTSE

Maximum catering time = +13.2 min.

### 6. GROUND HANDLING/GENERAL SERVICING

Start of operations:

- Bridges/stairs: t0 = 0.
- Other equipment t = t0.

GPU: up to 90 kVA.

Air conditioning: one hose.

Potable water servicing: 100% uplift, 200L.

Toilet servicing: draining and rinsing.

### 7. SECURITY/SAFETY CHECKS

No safety or security checks are applicable.

## GANTT CHART

Week	1	2	3	4	5	6	7	8	9	10	11
Start Date	25-Sep	02-Oct	09-Oct	16-Oct	23-Oct	30-Oct	06-Nov	13-Nov	20-Nov	27-Nov	04-Dec
<b>Initial Research</b>											
Requirement Identification	█										
Market Research	█	█									
<b>Initial Concept Design</b>											
Concept Creation		█	█								
Trade-off & Down-selection		█	█								
<b>Initial Sizing</b>											
Initial Sizing			█	█							
Review & Freeze			█	█							
<b>PDR</b>											
PDR Preparation				█							
PDR Deadline				X							
PEDR Preparation					█						
PEDR Deadline					X						
<b>Design Refinement</b>											
Sizing Iteration 1					█						
Sizing Iteration 2					X						
Sizing Iteration 3						█					
<b>FDR</b>											
FDR Preparation										█	█
FDR Deadline									X		
FEDR Preparation										█	█
FEDR Deadline									X		

Figure 48: Gantt chart of project

Table 26: Mission characteristics of each phase

Mission phase	170-variant			222-variant		
	Range	Time (min)	Fuel (kg)	Range	Time (min)	Fuel (kg)
Start of taxi-out	0.00	0.00	0.00	0.00	0.00	0.00
End of taxi-out / Start of take-off	0.00	7.00	214.26	0.00	7.00	214.26
End of take-off / Start of climb	0.00	0.82	272.29	0.00	0.86	285.64
End of climb / Start of cruise	198.73	28.67	1757.76	190.28	27.76	1792.19
End of 1st cruise step	2053.74	263.65	9876.48	2052.74	263.61	10343.73
End of 2nd step	3166.74	404.65	14747.71	3170.21	405.12	15474.65
End of 3rd step	3723.25	475.14	17183.33	3728.94	475.88	18040.11
End of 4th step / Start of descent	3908.75	498.64	17995.20	3915.19	499.46	18895.26
End of descent / Start of approach	92.53	15.16	77.31	94.53	15.48	78.86
End of approach / Start of taxi-in	0.00	5.00	296.78	0.00	5.00	251.83
End of taxi-in	0.00	7.00	163.02	0.00	7.00	163.02
Total	4200.00	562.29	20776.62	4200.00	562.56	21681.08
Reserves:						
Percentage policy reserves	0.00	16.45	599.36	0.00	16.46	629.06
Continued cruise reserves	0.00	45.00	1458.23	0.00	45.00	1515.70
End of overshoot / Start of climb	0.00	0.62	164.04	0.00	0.65	172.35
End of climb / Start of cruise	26.00	5.28	400.99	27.86	5.66	429.26
End of cruise / Start of descent	124.66	20.29	617.79	122.04	19.87	619.69
End of descent / Start of hold	49.34	10.19	57.63	50.10	10.34	58.52
End of hold / Start of approach	0.00	30.00	805.81	0.00	30.00	833.16
End of diversion approach	0.00	5.00	277.02	0.00	5.00	236.27
Total	4400.00	695.12	25157.48	4400.00	695.54	26175.10

## Structures

Table 27: Number of plies needed along the span for the wing box skin and spar

Distance from root (m)	Skin	Spar
0	94	188
0.5	91	182
1	87	175
1.5	84	169
2	78	163
2.5	75	156
3	71	150
3.5	68	143
4	65	137
4.1435	70	145
4.5	68	141
5	64	135
5.5	61	129
6	58	123
6.5	55	117
7	52	111
7.5	49	105
8	46	99
8.5	43	93
9	40	88
9.5	37	82
10	35	76
10.5	32	71
11	29	65
11.5	27	59
12	25	54
12.5	22	49
13	20	43
13.5	18	38
14	16	33
14.5	15	28
15	13	24
15.5	12	19
15.6983	11	22
16	10	20
16.5	9	16
17	8	13
17.5	7	10
18	7	8
18.5	6	6
18.515	6	6

## Fuel Systems

FUEL VOLUME CALCS							
TARGET							
Mission Fuel	27943	23649	Fuel Mass	<b>27943 kg</b>			
Reserves Fuel	0	4294.4	Fuel Volume	<b>34928.8 L</b>			
Wingbox to ch	0.55			<b>ONE WINGBOX</b>			
Panel 2	Value	Units	Panel 3	Value	Units	ACT	
Span	4.893	m	Span	10.807	m	Length	<b>3.34675 m</b>
Root Chord	3.34675	m	Root Chord	2.00805	m	Width	2.2 m
Tip Chord	2.00805	m	Tip Chord	0.93709	m	Thickness	<b>0.602415 m</b>
Root t/c	0.18		Root t/c	<b>0.14</b>		Volume	<b>4.435491283 m^3</b>
Tip t/c	<b>0.14</b>		Tip t/c	0.1		Volume	<b>4435.491283 L</b>
Root Thickness:	<b>0.60242</b>	m	Root Thickness	<b>0.28113</b>	m	LWD3-45W	
Tip Thickness	<b>0.28113</b>	m	Tip Thickness	<b>0.09371</b>	m	Volume	<b>3.5 m^3</b>
Volume	<b>5.78743</b>	m^3	Volume	<b>2.98258</b>	m^3	Volume	<b>3500 L</b>
Volume	<b>5787.43</b>	L	Volume	<b>2982.58</b>	L	Fuel Mass	
TWO WINGBOX AND ACT							
Total Volume	<b>26411</b>	L				Wing	<b>14032.01771 kg</b>
RCT	<b>8517.75</b>	L	# of RCT needed	2.5		ACT	<b>7096.786052 kg</b>
Assumed linear taper for simplification							
Trapezoidal Prism Volume Calc							
Wing Box Dimensions due to Control Surfaces							
Required						RCT	<b>6814.196235 kg</b>
						Total	<b>27943 kg</b>

Figure 49: Fuel Volume Analysis